A&A 520, A1 (2010)
DOI: 10.1051/0004-6361/200912983

Astronomy & Astrophysics
Special feature

Pre-launch status of the Planck mission

Planck pre-launch status: The *Planck* mission

J. A. Tauber[36], N. Mandolesi[45], J.-L. Puget[52], T. Banos[82], M. Bersanelli[32], F. R. Bouchet[51], R. C. Butler[45], J. Charra[52], G. Crone[37], J. Dodsworth[38], G. Efstathiou[90], R. Gispert[52], G. Guyot[52], A. Gregorio[93], J. J. Juillet[82], J.-M. Lamarre[66], R. J. Laureijs[36], C. R. Lawrence[61], H. U. Nørgaard-Nielsen[35], T. Passvogel[37], J. M. Reix[82], D. Texier[39], L. Vibert[52], A. Zacchei[46], P. A. R. Ade[6], N. Aghanim[52], B. Aja[18], E. Alippi[84], L. Aloy[37], P. Armand[82], M. Arnaud[7], A. Arondel[52], A. Arreola-Villanueva[61], E. Artal[18], E. Artina[84], A. Arts[37], M. Ashdown[89], J. Aumont[9], M. Azzaro[40], A. Bacchetta[83], C. Baccigalupi[5], M. Baker[37], M. Balasini[84], A. Balbi[33], A. J. Banday[67,12], G. Barbier[64], R. B. Barreiro[58], M. Bartelmann[67,95], P. Battaglia[84], E. Battaner[91], K. Benabed[51], J.-L. Beney[63], R. Beneyton[51], K. Bennett[36], A. Benoit[64], J.-P. Bernard[12], P. Bhandari[61], R. Bhatia[61], M. Biggi[74], R. Biggins[38], G. Billig[38], Y. Blanc[14], H. Blavot[52], J. J. Bock[61], A. Bonaldi[49], R. Bond[13], J. Bonis[63], J. Borders[61], J. Borrill[88], L. Boschini[84], F. Boulanger[52], J. Bouvier[64], M. Bouzit[52], R. Bowman[61], E. Bréelle[4], T. Bradshaw[77], M. Braghin[37], M. Bremer[36], D. Brienza[34], D. Broszkiewicz[4], C. Burigana[45], M. Burkhalter[73], P. Cabella[33], T. Cafferty[61], M. Cairola[83], S. Caminade[52], P. Camus[53], C. M. Cantalupo[65], B. Cappellini[32], J.-F. Cardoso[4], R. Carr[39], A. Catalano[4], L. Cayón[23], M. Cesa[83], M. Chaigneau[52], A. Challinor[90], A. Chamballu[43], J. P. Chambelland[82], M. Charra[52], L.-Y. Chiang[55], G. Chlewicki[83], P. R. Christensen[71], S. Church[24], E. Ciancietta[83], M. Cibrario[83], R. Cizeron[63], D. Clements[43], B. Collaudin[82], J.-M. Colley[4,51], S. Colombi[51], A. Colombo[37], F. Colombo[84], O. Corre[82], F. Couchot[63], B. Cougrand[52], A. Coulais[66], P. Couzin[82], B. Crane[52], B. Crill[61], M. Crook[77], D. Crumb[61], F. Cuttaia[45], U. Dörl[67], P. da Silva[51], R. Daddato[37], C. Damasio[37], L. Danese[5], G. d'Aquino[37], O. D'Arcangelo[60], K. Dassas[52], R. D. Davies[62], W. Davies[73], R. J. Davis[62], P. De Bernardis[34], D. de Chambure[37], G. de Gasperis[33], M. L. De la Fuente[18], P. De Paco[81], A. De Rosa[45], G. De Troia[33], G. De Zotti[49], M. Dehamme[63], J. Delabrouille[4], J.-M. Delouis[51], F.-X. Désert[64], G. di Girolamo[38], C. Dickinson[62], E. Doelling[38], K. Dolag[67], I. Domken[11], M. Douspis[52], D. Doyle[37], S. Du[63], D. Dubruel[82], C. Dufour[4], C. Dumesnil[52], X. Dupac[39], P. Duret[52], C. Eder[63], A. Elfving[37], T. A. Enßlin[67], P. Eng[52], K. English[61], H. K. Eriksen[10,56], P. Estaria[37], M. C. Falvella[2], F. Ferrari[84], F. Finelli[45], A. Fishman[61], S. Fogliani[46], S. Foley[38], A. Fonseca[61], G. Forma[82], O. Forni[12], P. Fosalba[87], J.-J. Fourmond[52], M. Frailis[46], C. Franceschet[32], E. Franceschi[45], S. François[52], M. Frerking[61], M. F. Gómez-Reñasco[57], K. M. Górski[61], T. C. Gaier[61], S. Galeotta[48], K. Ganga[4], J. García Lázaro[39], A. Garnica[61], M. Gaspard[63], E. Gavila[82], M. Giard[12], G. Giardino[36], G. Gienger[38], Y. Giraud-Heraud[4], J.-M. Glorian[12], M. Griffin[6], A. Gruppuso[45], L. Guglielmi[4], D. Guichon[82], B. Guillaume[37], P. Guillouet[4], J. Haissinski[63], F. K. Hansen[10,56], J. Hardy[61], D. Harrison[90], A. Hazell[76], M. Hechler[38], V. Heckenauer[52], D. Heinzer[38], R. Hell[67], S. Henrot-Versillé[63], C. Hernández-Monteagudo[67], D. Herranz[58], J. M. Herreros[57], V. Hervier[52], A. Heske[37], A. Heurtel[63], S. R. Hildebrandt[57], R. Hills[89], E. Hivon[51], M. Hobson[89], D. Hollert[61], W. Holmes[61], A. Hornstrup[35], W. Hovest[67], R. J. Hoyland[57], G. Huey[61], K. M. Huffenberger[92], N. Hughes[94], U. Israelsson[61], B. Jackson[37], A. Jaffe[43], T. R. Jaffe[62], T. Jagemann[39], N. C. Jessen[35], J. Jewell[61], W. Jones[22], M. Juvela[72], J. Kaplan[4], P. Karlman[61], F. Keck[38], E. Keihänen[21], M. King[61], T. S. Kisner[65], P. Kletzkine[37], R. Kneissl[67], J. Knoche[67], L. Knox[26], T. Koch[61], M. Krassenburg[37], H. Kurki-Suonio[21,42], A. Lähteenmäki[68], G. Lagache[52], E. Lagorio[64], P. Lami[52], J. Lande[12], A. Lange[61], F. Langlet[52], R. Lapini[74], M. Lapolla[84], A. Lasenby[89], M. Le Jeune[4], J. P. Leahy[62], M. Lefebvre[52], F. Legrand[51], G. Le Meur[63], R. Leonardi[27], B. Leriche[52], C. Leroy[52], P. Leutenegger[84], S. M. Levin[61], P. B. Lilje[10,56], C. Lindensmith[61], M. Linden-Vørnle[86], A. Loc[61], Y. Longval[52], P. M. Lubin[27], T. Luchik[61], I. Luthold[37], J. F. Macias-Perez[96], T. Maciaszek[14], C. MacTavish[43], S. Madden[37], B. Maffei[62], C. Magneville[8], D. Maino[32], A. Mambretti[84], B. Mansoux[63], D. Marchioro[84], M. Maris[46], F. Marliani[37], J.-C. Marrucho[63], J. Martí-Canales[37], E. Martínez-González[58], A. Martín-Polegre[37], P. Martin[82], C. Marty[12], W. Marty[12], S. Masi[34], M. Massardi[49], S. Matarrese[31], F. Matthai[67], P. Mazzotta[33], A. McDonald[38], P. McGrath[61], A. Mediavilla[18], P. R. Meinhold[27], J.-B. Mélin[8], F. Melot[96], L. Mendes[39], A. Mennella[32], C. Mervier[52], L. Meslier[52], M. Miccolis[84], M.-A. Miville-Deschenes[52], A. Moneti[51], D. Montet[82], L. Montier[12], J. Mora[61], G. Morgante[45], G. Morigi[45], G. Morinaud[52], N. Morisset[59], D. Mortlock[90], S. Mottet[51], J. Mulder[61], D. Munshi[90], A. Murphy[70], P. Murphy[61], P. Musi[83], J. Narbonne[12], P. Naselsky[71], A. Nash[61], F. Nati[34], P. Natoli[33], B. Netterfield[13], J. Newell[61], M. Nexon[12], C. Nicolas[52], P. H. Nielsen[85], N. Ninane[11], F. Noviello[52], D. Novikov[43], I. Novikov[71], I. J. O'Dwyer[61], P. Oldeman[37], P. Olivier[37], L. Ouchet[82], C. A. Oxborrow[35], L. Pérez-Cuevas[37], L. Pagan[84], C. Paine[61], F. Pajot[52], R. Paladini[80], F. Pancher[64], J. Panh[14], G. Parks[61], P. Parnaudeau[51], B. Partridge[41], B. Parvin[61], J. P. Pascual[18], F. Pasian[46], D. P. Pearson[61], T. Pearson[61], M. Pecora[84], O. Perdereau[63], L. Perotto[96], F. Perrotta[5], F. Piacentini[34], M. Piat[4], E. Pierpaoli[20], O. Piersanti[37], E. Plaige[63], S. Plaszczynski[63], P. Platania[60], E. Pointecouteau[12], G. Polenta[1], N. Ponthieu[52], L. Popa[54], G. Poulleau[52], T. Poutanen[21,42,68], G. Prézeau[61], L. Pradell[16], M. Prina[61], S. Prunet[51], J. P. Rachen[67], D. Rambaud[12], F. Rame[83], I. Rasmussen[37], J. Rautakoski[37], W. T. Reach[50], R. Rebolo[57], M. Reinecke[67], J. Reiter[61], C. Renault[96], S. Ricciardi[79], P. Rideau[82], T. Riller[67], I. Ristorcelli[12], J. B. Riti[82], G. Rocha[61], Y. Roche[82], R. Pons[12], R. Rohlfs[59], D. Romero[61], S. Roose[11], C. Rosset[63], S. Rouberol[51], M. Rowan-Robinson[43], J. A. Rubiño-Martín[57], P. Rusconi[84], B. Rusholme[50], M. Salama[61], E. Salerno[15], M. Sandri[45], D. Santos[96], J. L. Sanz[58], L. Sauter[51], F. Sauvage[82], G. Savini[75], M. Schmelzel[61], A. Schnorhk[37], W. Schwarz[61], D. Scott[19], M. D. Seiffert[61], P. Shellard[89], C. Shih[61], M. Sias[83], J. I. Silk[29], R. Silvestri[84], R. Sippel[3], G. F. Smoot[25], J.-L. Starck[8], P. Stassi[96], J. Sternberg[36], F. Stivoli[79], V. Stolyarov[90], R. Stompor[4], L. Stringhetti[45], D. Strommen[61], T. Stute[3], R. Sudiwala[6], R. Sugimura[61], R. Sunyaev[67], J.-F. Sygnet[51], M. Türler[59], E. Taddei[84], J. Tallon[61], C. Tamiatto[52], M. Taurigna[63], D. Taylor[39], L. Terenzi[45], S. Thuerey[37], J. Tillis[61], G. Tofani[44], L. Toffolatti[17], E. Tommasi[2], M. Tomasi[32], E. Tonazzini[15], J.-P. Torre[52], S. Tosti[52], F. Touze[63], M. Tristram[63], J. Tuovinen[69], M. Tuttlebee[38], G. Umana[47], L. Valenziano[45], D. Vallée[4], M. van der Vlis[37], F. Van Leeuwen[90], J.-C. Vanel[4], B. Van-Tent[51], J. Varis[69], E. Vassallo[38], C. Vescovi[64], F. Vezzu[64], D. Vibert[51], P. Vielva[58], J. Vierra[61], F. Villa[45], N. Vittorio[33], C. Vuerli[46], L. A. Wade[61], A. R. Walker[19], B. D. Wandelt[28], C. Watson[38], D. Werner[38], M. White[30], S. D. M. White[67], A. Wilkinson[62], P. Wilson[61], A. Woodcraft[6], B. Yoffo[4], M. Yun[61], V. Yurchenko[70], D. Yvon[8], B. Zhang[61], O. Zimmermann[64], A. Zonca[48], and D. Zorita[78]

(Affiliations can be found after the references)

Received 24 July 2009 / Accepted 12 November 2009

ABSTRACT

The European Space Agency's *Planck* satellite, launched on 14 May 2009, is the third-generation space experiment in the field of cosmic microwave background (CMB) research. It will image the anisotropies of the CMB over the whole sky, with unprecedented sensitivity ($\frac{\Delta T}{T} \sim 2 \times 10^{-6}$) and angular resolution (~5 arcmin). *Planck* will provide a major source of information relevant to many fundamental cosmological problems and will test current theories of the early evolution of the Universe and the origin of structure. It will also address a wide range of areas of astrophysical research related to the Milky Way as well as external galaxies and clusters of galaxies. The ability of *Planck* to measure polarization across a wide frequency range (30–350 GHz), with high precision and accuracy, and over the whole sky, will provide unique insight, not only into specific cosmological questions, but also into the properties of the interstellar medium. This paper is part of a series which describes the technical capabilities of the *Planck* scientific payload. It is based on the knowledge gathered during the on-ground calibration campaigns of the major subsystems, principally its telescope and its two scientific instruments, and of tests at fully integrated satellite level. It represents the best estimate before launch of the technical performance that the satellite and its payload will achieve in flight. In this paper, we summarise the main elements of the payload performance, which is described in detail in the accompanying papers. In addition, we describe the satellite performance elements which are most relevant for science, and provide an overview of the plans for scientific operations and data analysis.

Key words. cosmic microwave background – space vehicles: instruments – instrumentation: detectors – instrumentation: polarimeters – submillimeter: general – radio continuum: general

1. Introduction

The *Planck* mission[1] was conceived in 1992, in the wake of the release of the results from the COsmic Background Explorer (COBE) satellite (Boggess et al. 1992), notably the measurement by the FIRAS instrument of the shape of the spectrum of the cosmic microwave background (CMB), and the detection by the DMR instrument of the spatial anisotropies of the temperature of the CMB. The latter result in particular led to an explosion in the number of ground-based and suborbital experiments dedicated to mapping of the anisotropies, and to proposals for space experiments both in Europe and the USA.

The development of *Planck* began with two proposals presented to the European Space Agency (ESA) in May of 1993, for the COsmic Background Radiation Anisotropy Satellite (COBRAS, Mandolesi et al. 1993) and the SAtellite for Measurement of Background Anisotropies (SAMBA, Puget et al. 1993). Each of these proposed a payload formed by an offset Gregorian telescope focussing light from the sky onto an array of detectors (based on high electron mobility transistor [HEMT] low noise amplifiers for COBRAS and very low temperature bolometers for SAMBA) fed by corrugated horns. The two proposals were used by an ESA-led team to design a payload where a single COBRAS-like telescope fed two instruments, a COBRAS-like Low Frequency Instrument (LFI), and a SAMBA-like High Frequency Instrument (HFI) sharing a common focal plane. A period of study of this concept culminated in the selection by ESA in 1996 of the COBRAS/SAMBA satellite (described in the so-called "Redbook", Bersanelli et al. 1996) into its programme of scientific satellites. At the time of selection the launch of COBRAS/SAMBA was expected to be in 2003. Shortly after the mission was approved, it was renamed in honor of the German scientist Max Planck (1858–1947), winner of the Nobel Prize for Physics in 1918.

Shortly after its selection, the development of *Planck* was joined with that of ESA's *Herschel* Space Telescope, based on a number of potential commonalities, the most important of which was that both missions targeted orbits around the second Lagrangian point of the Sun-Earth system and could therefore share a single heavy launcher. In practice the joint development has meant that a single ESA engineering team has led the development of both satellites by a single industrial prime contractor, leading to the use of many identical hardware and software subsystems in both satellites, and a synergistic sharing of engineering skills and manpower. The industrial prime contractor, Thales Alenia Space France, was competitively selected in early 2001. Thales Alenia Space France was supported by two major subcontractors: Thales Alenia Space Italy for the service module of both *Planck* and *Herschel*, and EADS Astrium GmbH for the *Herschel* payload module, and by many other industrial subcontractors from all ESA member states. The development of the satellite has been regularly reported over the years, see e.g. Reix et al. (2007).

In early 1999, ESA selected two consortia of scientific institutes to provide the two *Planck* instruments which were part of the payload described in the Redbook: the LFI was developed by a consortium led by N. Mandolesi of the Istituto di Astrofisica Spaziale e Fisica Cosmica (CNR) in Bologna (Italy); and the HFI by a consortium led by J.-L. Puget of the Institut d'Astrophysique Spatiale (CNRS) in Orsay (France). More than 40 European institutes, and some from the USA, have collaborated on the development and testing of these instruments, and will continue to carry out their operation, as well as the ensuing data analysis and initial scientific exploitation (see also Appendix A).

In early 2000, ESA and the Danish National Space Institute (DNSI) signed a Letter of Agreement for the provision of the two reflectors that are used in the *Planck* telescope. DNSI led a consortium of Danish institutes, which together with ESA subcontracted the development of the *Planck* reflectors to EADS Astrium GmbH (Friedrichshafen, D), who have manufactured the reflectors using state-of-the-art carbon fibre technology.

The long development history of the *Planck* satellite (see Fig. 1) culminated with its successful launch on 14 May 2009.

This paper is not meant to describe in detail *Planck*'s scientific objectives or capabilities. A detailed and still quite up-to-date description of the *Planck* mission and, more specifically, of its scientific objectives was produced in 2005, the "Planck Bluebook" (*Planck* Collaboration 2005). This paper is meant to provide an update to the technical description of the payload in the Planck Bluebook, summarising the best knowledge available at the time of launch of the major scientifically relevant performance elements of the satellite and its payload, based on all the ground testing activities and extrapolation to flight conditions. It is part of a set of papers which details the payload performance and which will be referred to whenever

[1] *Planck* (http://www.esa.int/Planck) is a project of the European Space Agency – ESA – with instruments provided by two scientific Consortia funded by ESA member states (in particular the lead countries: France and Italy) with contributions from NASA (USA), and telescope reflectors provided in a collaboration between ESA and a scientific Consortium led and funded by Denmark.

Fig. 1. The fully assembled *Planck* satellite a few days before integration into the Ariane 5 rocket. *Herschel* is visible by reflection on the primary reflector. Photo by A. Arts.

possible for detailed descriptions. In addition to a summary of the material presented in the accompanying papers, this one also includes a description of the scientifically relevant elements of the satellite performance, of its planned operations, and a brief overview of the "science ground segment". The main accompanying papers, most of which are part of this special issue of *Astronomy & Astrophysics*, include:

- Tauber et al. (2010), describing the optical performance of the combined payload, i.e. telescope plus instruments;
- Mandolesi et al. (2010), describing programmatic aspects of the LFI and its development;
- Bersanelli et al. (2010), describing in detail the design of the LFI;
- Mennella et al. (2010), describing the test and calibration programme of the LFI at instrument and system levels prior to launch;
- Villa et al. (2010), describing the test and calibration of the LFI radiometer chains;
- Sandri et al. (2010), describing the design and test of the LFI optics;
- Leahy et al. (2010), describing the polarisation aspects of the LFI, and its expected performance in orbit;
- Lamarre et al. (2010), describing in detail the on-ground design, manufacture, test and performance of the HFI;
- Pajot et al. (2010), describing the test and calibration programme of the HFI prior to launch;
- Ade et al. (2010), describing the design, test and performance of the cryogenic elements of the HFI focal plane;
- Holmes et al. (2008), describing the design, manufacture and test of the HFI bolometers;
- Maffei et al. (2010), describing the design and test of the HFI optics;
- Rosset et al. (2010), describing the polarisation aspects of the HFI.

2. Satellite description

Figures 2 and 3 show the major elements and characteristics of the *Planck* satellite. *Planck* was designed, built and tested around two major modules:

1. a *payload module* (see Fig. 5) containing an off-axis telescope with a projected diameter of 1.5 m, focussing radiation from the sky onto a focal plane shared by detectors of the LFI and HFI, operating at 20 K and 0.1 K respectively; a telescope baffle that simultaneously provides stray-light shielding and radiative cooling; and three conical "V-groove" baffles that provide thermal and radiative insulation between the warm *service module* and the cold telescope and instruments.
2. a *service module* (see Fig. 6) containing all the warm electronics servicing instruments and satellite; and the solar panel providing electrical power. It also contains the cryocoolers, the main on-board computer, the telecommand receivers and telemetry transmitters, and the attitude control system with its sensors and actuators.

The most relevant technical characteristics of the *Planck* spacecraft are detailed in Table 1.

2.1. Pointing

Planck spins at 1 rpm around the axis of symmetry of the solar panel[2]. In flight, the solar panel can be pointed within a cone of 10° around the direction to the Sun; everything else is always in its shadow. The attitude control system relies principally on:

- Redundant star trackers as main sensors, and solar cells for rough guidance and anomaly detection. The star trackers contain CCDs which are read out in synchrony with the speed of the field-of-view across the sky to keep star images compact.
- Redundant sets of hydrazine 20 N thrusters for large manoeuvers and 1 N thrusters for fine manoeuvers.

An on-board computer dedicated to this task reads out the star trackers at a frequency of 4 Hz, and determines in real time the absolute pointing of the satellite based on a catalogue of bright stars. Manoeuvers are carried out as a sequence of 3 or 4 thrusts spaced in time by integer spin periods, whose duration is calculated on-board, with the objective to achieve the requested attitude with minimal excitation of nutation. There is no further active damping of nutation during periods of inertial pointing, i.e. between manoeuvers. The duration of a small manoeuver typical of routine operations (2 arcmin) is ~5 min. Larger manoeuvers are achieved by a combination of thrusts using both 1 N and 20 N thrusters, and their duration can be considerable (up to several hours for manoeuver amplitudes of several degrees). The attitudes measured on-board are further filtered on the ground to reconstruct with high accuracy the spacecraft attitude (or rather the star tracker reference frame). The star trackers and the instrumental field-of-view were aligned on the ground independently to the spacecraft reference frame; the resulting alignment accuracy between the star trackers and the instruments was of

[2] In reality, *Planck* spins about its principal axis of inertia, which does not coincide exactly with the geometrical axis; this difference will evolve slowly during the mission due to fuel expenditure. After on-ground balancing, the difference (often called "wobble angle") is predicted to be ~–14 arcmins just after launch (mainly around the *Y* axis, see Fig. 3), and to vary between ~–5 arcmins after the final injection manoeuver into L2 (when most of the fuel has been expended), to ~+5 arcmin at end of the nominal mission lifetime.

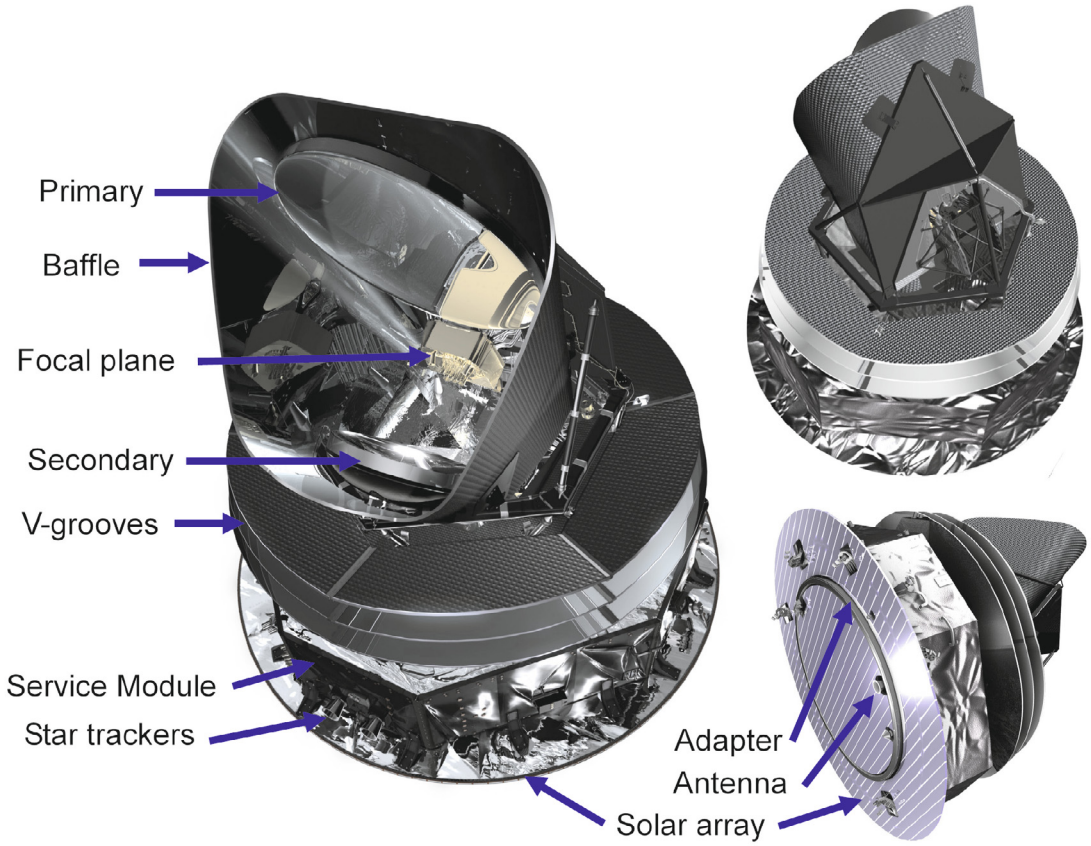

Fig. 2. An artist's impression of the main elements of *Planck*. The instrument focal plane unit (barely visible, see Fig. 4) contains both LFI and HFI detectors. The function of the large baffle surrounding the telescope is to control the very-far-sidelobe level of the radiation pattern as seen from the detectors, and it also contributes substantially to radiative cooling of the payload. The specular conical shields (often called "V-grooves") thermally decouple the octagonal service module (which contains all warm elements of the satellite) from the payload module. The clampband adapter which holds the satellite to the rocket, and the medium-gain horn antenna used to transmit science data to ground are also indicated.

0.°19, far better than required. The angles between the star tracker frame and each of the detectors are determined in flight from observations of planets. Several bright planets drift through the field-of-view once every 6 months, providing many calibration points every year. There are many weaker point sources, both celestial and in the Solar System, which provide much more frequent though less accurate calibration tests. The in-flight pointing calibration is very robust vis-à-vis the expected thermoelastic deformations (which contribute a total of 0.14 arcmin to the total on-ground alignment budget). The most important pointing performance aspects, based on a realistic simulation using rather conservative parameter values, and tests of the attitude control system, are summarised in Table 2.

The 20 N thrusters are also used for orbit control manoeuvers during transfer to the final *Planck* orbit (two large manoeuvers planned) and for orbit maintenance (typically one manoeuver per month). Most of the hydrazine thruster fuel that *Planck* carries is expended in the two large manoeuvers carried out during transfer, and a very minor amount is required for orbit maintenance.

2.2. Thermal design and the cryo-chain

The cryogenic temperatures required by the detectors are achieved through a combination of passive radiative cooling and three active refrigerators. The contrast between the high power dissipation in the warm service module (~1000 W at 300 K) and that at the coldest spot in the satellite (~100 nW at 0.1 K) are testimony to the extraordinary efficiency of the complex thermal system which has to achieve such disparate ends simultaneously while preserving a very high level of stability at the cold end.

The telescope baffle and V-groove shields (see Fig. 2) are key parts of the passive thermal system. The baffle (which also acts as a stray-light shield) is a high-efficiency radiator consisting of ~14 m^2 of open aluminium honeycomb coated with black cryogenic paint; the effective emissivity of this combination is very high (>0.9). The "V-grooves" are a set of three conical shields with an angle of 5° between adjacent shields; the surfaces (approx 10 m^2 on each side) are specular (aluminum coating with an emissivity of ~0.045) except for the outer (~4.5 m^2) area of the topmost V-groove which has the same high-emissivity coating as the baffle. This geometry provides highly efficient radiative coupling to cold space, and a high degree of thermal and radiative isolation between the warm spacecraft bus and the cold telescope, baffle, and instruments. The cooling provided by the passive system leads to a temperature of 40–45 K for the telescope and baffle. Table 3 lists temperature ranges predicted in flight for various parts of the satellite, based on a thermo-mechanical model which has been correlated to test results; the uncertainty in the prediction for elements in the cold payload is of order (+0.5 K, −2 K).

The active refrigeration chain further reduces the detector temperatures to 20 K (LFI front-end low noise amplifiers) and 0.1 K (HFI bolometers) respectively. It is based on three distinct units working in series (see Fig. 7):

1. The hydrogen **sorption cooler** was designed and built expressly for *Planck* at NASA's Jet Propulsion Laboratory

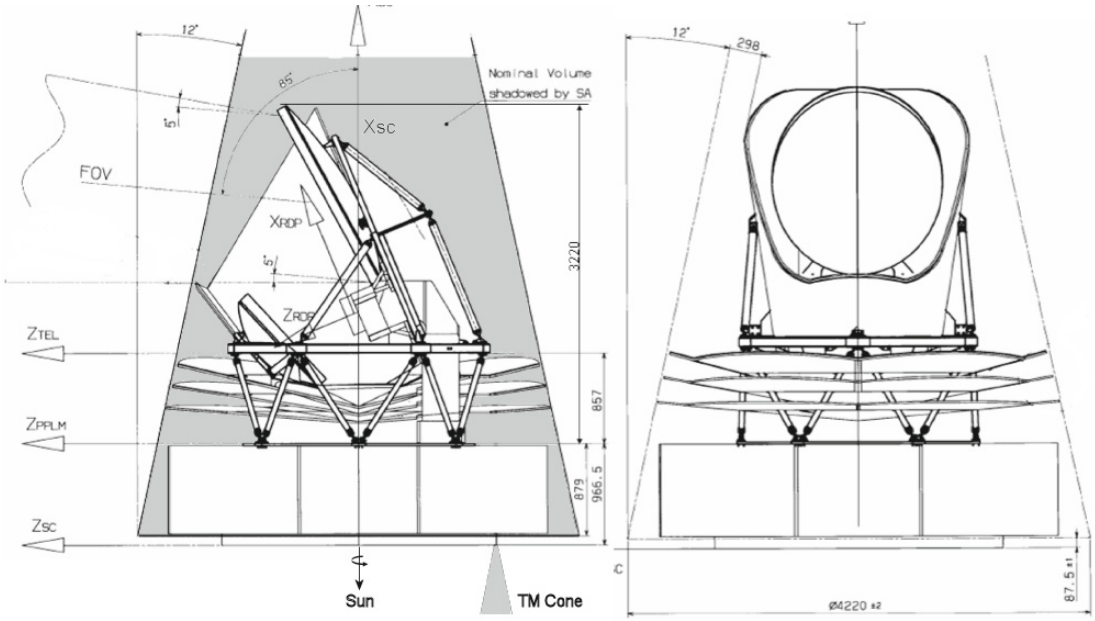

Fig. 3. Engineering cross-sectional diagrams of *Planck* show its overall dimensions (in mm). The satellite spins around the vertical axis (+X), such that the solar array is always exposed to the Sun, and shields the payload from solar radiation. The shadow cone (±10°) is indicated in *the left panel*; the TM cone (±15°), i.e. the angle within which the medium-gain data transmission link to Earth can be maintained, is also indicated. Figures courtesy of Thales Alenia Space (France).

Table 1. *Planck* satellite characteristics.

Diameter	4.2 m	Defined by the solar array
Height	4.2 m	
Total mass at launch	1912 kg	Fuel mass = 385 kg at launch; He mass = 7.7 kg
Electrical power demand (avg)	1300 W	Instrument part: 685 W (Begining of Life), 780 W (End of Life)
Operational lifetime	18 months	Plus a possible extension of one year
Spin rate	1 rpm	±0.6 arcmin/sec (changes due to manoeuvers)
		Stability during inertial pointing $\sim 6.5 \times 10^{-5}$ rpm/h
Max angle of spin axis to Sun	10°	To maintain the payload in the shade. Default angle is 7.5.
Max angle of spin axis to Earth	15°	To allow communication to Earth
Angle between spin axis and telescope boresight	85°	Max extent of FOV ~ 8°
On-board data storage capacity	32 Gbit	Two redundant units (only one is operational at any time)
Data transmission rate to ground (max)	1.5 Mbps	Within 15° of Earth, using a 35 m ground antenna
Daily contact period	3 h	The effective real-time science data acquisition bandwidth is 130 kbps.

(USA) (Bhandari et al. 2004; Pearson et al. 2006); it directly cools the LFI low-noise amplifiers to their operating temperature while providing pre-cooling for the HFI cooler chain. The sorption cooler consists of two cold redundant units, each including a six-element sorption compressor and a Joule-Thomson (JT) expansion valve. Each element of the compressor is filled with hydride material ($La\ Ni_{4.78}\ Sn_{0.22}$) which alternately absorbs and releases hydrogen gas under control of a heat source. The cooler produces liquid hydrogen in two liquid-vapor heat-exchangers (LVHXs) whose temperatures are stabilized by hydrogen absorption into three compressor elements. LVHX1 provides pre-cooling for the HFI 4K cooler, while LVHX2 cools the LFI focal plane unit (FPU). The vapor pressure of the liquid hydrogen in the LVHXs is determined primarily by the absorption isotherms of the hydride material used in the compressor elements. Thus, the heat rejection temperature of the compressor elements determines the instrument temperatures. On the spacecraft the compressor rejects heat to a radiator to space with flight allowable temperatures between 262 and 282 K; the radiator is a single unit which couples the active and redundant sorption coolers via a network of heat pipes. The operating efficiency of the *Planck* sorption cooler depends on passive cooling by radiation to space, which is accomplished by heat exchange of the gas piping to the three V-groove radiators. The final V-groove is required to be between 45 and 60 K to provide the required cooling power for the two instruments. At the expected operating temperature of ~47 K, with a working pressure of 3.2 MPa, the two sorption coolers produce the 990 mW of required cooling power for the two instruments, with a margin of ~100 mW. The temperature in flight at the heat exchangers will be 17.5 K (LVHX1) and 19 K (LVHX2). LVHX2 is actively stabilised by a closed loop heat control; typical temperature fluctuation spectra are shown in Fig. 8.

2. **The 4 K cooler** is based on the closed circuit JT expansion of helium, driven by two mechanical compressors, one for the high pressure side and one for the low pressure side. A description of this system is given in Bradshaw et al. (1997). Similar compressors have already been used for active cooling at 70 K in space. The *Planck* 4 K cooler was initially developed under an ESA programme to provide 4 K cooling

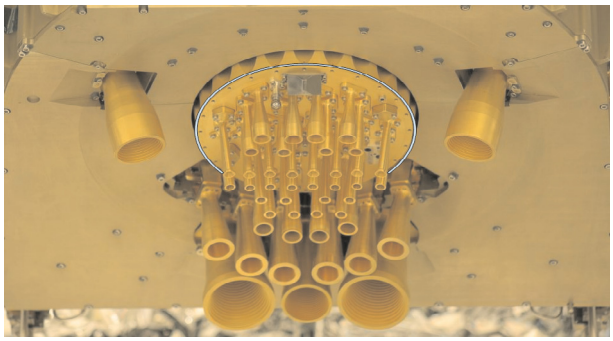

Fig. 4. *Planck* focal plane unit. The HFI array of feedhorns (identified by the blue circle) is located inside the ring formed by the LFI feed horns. The LFI focal plane structure (temperature 20 K) is attached by bipods to the telescope structure (temperature ~40 K). Thermally isolating bipods are also used to mechanically mount the HFI external structure (temperature 4 K) to the LFI focal plane. The externally visible HFI horns are at a temperature of 4 K; behind the first horn is a second stage at 1.6 K containing filters, and behind these the bolometer mounts at 0.1 K.

with reduced vibration for the FIRST (now *Herschel*) satellite. For this reason the two compressors are mounted in a back-to-back configuration, which cancels most of the momentum transfer to the spacecraft. Furthermore, force transducers placed between the two compressors provide an error signal which is used by the drive electronics servo system to control the motion profile of the pistons up to the 7th harmonic of the base compressor frequency (~40 Hz). The damping of vibration achieved by this system is more than two orders of magnitude at the base frequency and factors of a few at higher harmonics; the residual vibration levels will have a minor heating effect on the 100 mK stage, and negligible impact on the pointing. Pre-cooling of the helium is provided by the sorption cooler described above. The cold end of the cooler consists of a liquid helium reservoir located just behind the JT orifice. This cold tip is attached to the bottom of the 4 K box of the HFI FPU (see Fig. 7). It provides cooling for this screen and also pre-cooling for the gas in the dilution cooler pipe described later in this section. The margin between heat lift and heat load depends sensitively on the pre-cooling temperature provided by the sorption cooler at the LVHX1 interface. The temperature of LVHX1 is thus the most critical interface of the HFI cryogenic chain; system-level tests have shown that it is likely to be ~17.5 K, about 2 K below the maximum requirement[3]. At this pre-cooling temperature the heat load is 10.6 mW and the heat lift is 16.1 mW for a compressor stroke amplitude of 3.5 mm (the maximum is 4.4 mm). The heat load of the 4 K cooler onto the sorption cooler is only 30 mW, a very small amount with respect to the heat lift of the sorption cooler (990 mW); thus there is little back reaction of the 4 K onto the sorption cooler.

3. **The dilution cooler** consists of two cooling stages in series, using 36 000 litres of Helium 4 and 12 000 litres of Helium 3 gas stored on-board in 4 high-pressure tanks. The first stage is based on JT expansion, and produces cooling for the 1.6 K screen of the FPU and for pre-cooling of the second stage cooler. The latter is based on a dilution cooler principle working at zero-G, which was invented and tested by A. Benoît (Benoît et al. 1997), and developed into a

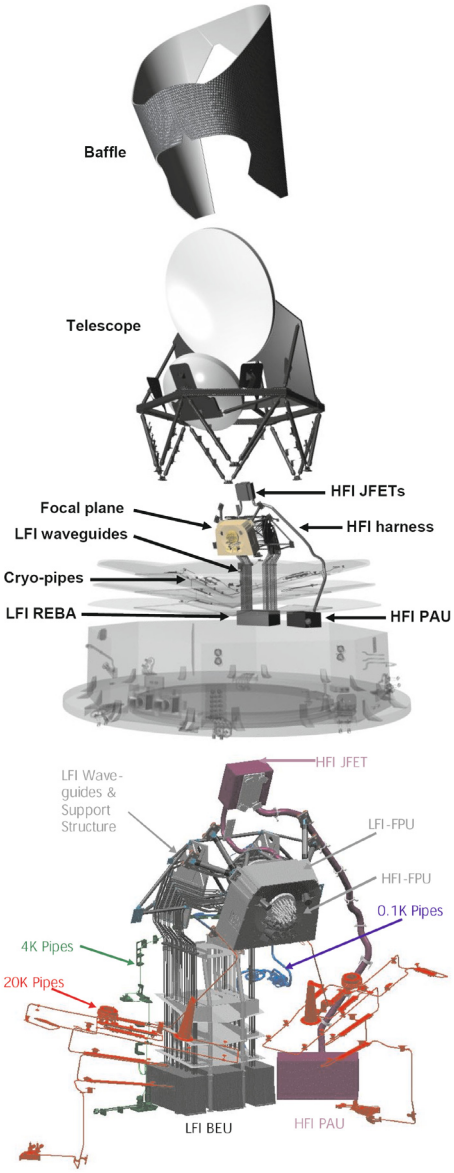

Fig. 5. *The upper panel* shows an exploded view of the *Planck* payload module. The baffle is made of aluminum honeycomb, externally open and coated with high emissivity paint, and internally covered with aluminum foil. The telescope support structure, made from carbon fiber reinforced plastic, consists mainly of a hexagonal frame and a large panel supporting the primary reflector. Twelve glass fiber reinforced plastic struts support the telescope frame and the three V-grooves. The grooves are facetted with six flat sectors of 60° each, made of aluminum sandwich with pure aluminum skins. The pipes carrying cryogenic fluid for the coolers are heat sunk onto each of the three V-grooves; a more detailed view of the piping can be seen in the lower panel. The focal plane is supported by three bipods to the primary reflector panel. Waveguides connect each LFI radiometer front-end amplifier to corresponding back-end amplifiers, located in the REBA (radiometer electronics and back-end assembly). The HFI bolometer signals are first processed by JFETs (junction-gate field effect transistors) operated at 130 K, and then amplified in the PAU (pre-amplifier unit). All further instrument electronic units are located inside the service module (see Fig. 6). Figures courtesy of ESA and Thales Alenia Space.

[3] The temperature of the cold end of the sorption cooler is mostly driven by that of the warm radiator on the satellite, which will be operated at 272 K (±10 K), leading to a temperature at LVHX1 of 17.5 K (±0.5). The warm radiator temperature is thus also a critical parameter, which can be kept in flight within the desired range as demonstrated during ground tests.

Table 2. *Planck* pointing performance.

Small manoeuver accuracy	<0.4 arcmin	1σ
Residual nutation after manoeuver	<0.85 arcmin	1σ
Drift during inertial pointing	2.5–3.5 arcmin/24 h	due to solar radiation pressure
Accuracy of on-ground determination of star tracker frame	<0.07 arcmin	1σ, at 8 Hz
Star-tracker to detector bias determination accuracy	~5 arcsec	1σ, based on simulations of planet obervations

space-qualified system by the Institut d'Astrophysique Spatiale (Orsay) and DTA Air Liquide (Grenoble), see Triqueneaux et al. (2006). The gas from the tanks (at 300 bars at the start of the mission) is brought down to 19 bars through a pressure regulator and the flow through the dilution is regulated by a set of discrete restrictions which can be switched by telecommand. The gas is vented to space after the dilution process[4], and the cooler therefore has a lifetime limited by the gas supply. The dilution of the two helium isotopes provides the cooling of the bolometers to a temperature around 100 mK which is required to deliver a very high sensitivity for the channels near the peak of the CMB spectrum (noise equivalent power around 10^{-17} W/ $\sqrt{\text{Hz}}$), limited mostly by the background photon noise.

A detailed description of the cooling system and its performance in flight will be prepared and published after the in-flight performance verification phase.

Table 3. *Planck* temperature ranges[a].

Element	$T_{\min}$ (K)	$T_{\max}$ (K)
Solar cells	378	382
Service module radiators	251	290
Sorption cooler warm radiator (active control)	262	280
Multi-layer insulation on Solar array	304	316
Multi-layer insulation on top of service module	198	287
Lower V-groove	111.9	152.6
Middle V-groove	76.4	91.6
Top V-groove	43.7	49.1
Sorption cooler interface on Top V-groove	44 (red.)	45.3 (nom.)
Primary reflector panel	38.3	43.8
Primary reflector	39.8	41.5
Secondary reflector	42.9	43.2
Baffle	42.3	44.0

Notes. [(a)] For each element listed, the min and max temperatures correspond to the coldest and warmest node in a thermal finite element model which has been correlated to the results of ground tests, when the model is run in a flight-like environment.

2.3. Instruments

The LFI (Bersanelli et al. 2010) is designed around 22 pseudo-correlation radiometers fed by corrugated feedhorns and orthomode transducers to separate two orthogonal linear polarisations. Each horn thus feeds two radiometers. The radiometers are based on front-end low noise amplifiers using indium-phosphide high electron mobility transistors, which process simultaneously the signal from the sky fed by the telescope, and the signal from stable blackbody reference loads located on the external body of the HFI where they can be maintained at a temperature of 4 K. The front-end amplifiers are located in the focal plane of the telescope, and are operated at a temperature of ~20 K; they feed warm back-end amplifiers and detection electronics via waveguides connecting the FPU to the warm service module. For each radiometer, sky and load time-ordered data are separately reconstructed and made available for processing on the ground. A detailed description of the LFI design and performance as measured on the ground are included in Bersanelli et al. (2010), Mennella et al. (2010), and other papers included in this issue.

The HFI (Lamarre et al. 2010) is designed around 52 bolometers fed by corrugated feedhorns and bandpass filters within a back-to-back conical horn optical waveguide. Twenty of the bolometers (spider-web bolometers or SWBs) are sensitive to total power, and the remaining 32 units are arranged in pairs of orthogonally-oriented polarisation-sensitive bolometers (PSBs). All bolometers are operated at a temperature of ~0.1 K, and read out by an AC-bias scheme through JFET amplifiers operated at ~130 K. Detailed descriptions of the HFI design and performance as measured on the ground are included in Lamarre et al. (2010), Pajot et al. (2010), and other papers included in this issue.

[4] The resulting pointing drift is negligible compared to other sources such as solar radiation pressure.

The frequency range of the two instruments together is designed to cover the peak of the CMB spectrum and to characterize the spectra of the main Galactic foregrounds (synchrotron and free-free emission at low frequencies, and dust emission at high frequencies). The LFI covers 30–70 GHz in three bands, and the HFI covers 100–857 GHz in six bands. The band centers are spaced approximately logarithmically. The main performance parameters of the instruments, as derived from ground testing, are summarized in Table 4.

In addition to the basic properties of each detector (Table 4), it is important to quantify their stability at various timescales, and the presence of non-white noise in the detector noise spectrum. These are described in the following sections.

2.3.1. Deviations from ideality in LFI

The LFI differential pseudo-correlation receiver scheme was designed to maximise stability and immunity to systematic effects of thermal or electrical origin (Bersanelli et al. 2010). The main sources of potential instabilities in the LFI signal are enumerated and briefly discussed below.

1. *Low frequency noise intrinsic to the radiometers* – HEMT low noise amplifiers, such as those used by LFI, exhibit gain and noise temperature fluctuations caused by the presence of traps in the semiconductor, resulting in a characteristic power spectral density $P(f) \propto 1/f^{\beta}$ with $\beta \approx 1$ ("$1/f$ noise"). The noise power spectral density of the LFI post-detection differenced signal is well described by:

$$P(f) \approx \sigma^2 \left[1 + \left(\frac{f_k}{f}\right)^{\beta}\right], \quad (1)$$

where σ^2 is the white noise limit and f_k is the characteristic knee-frequency. Test results on the LFI show typical

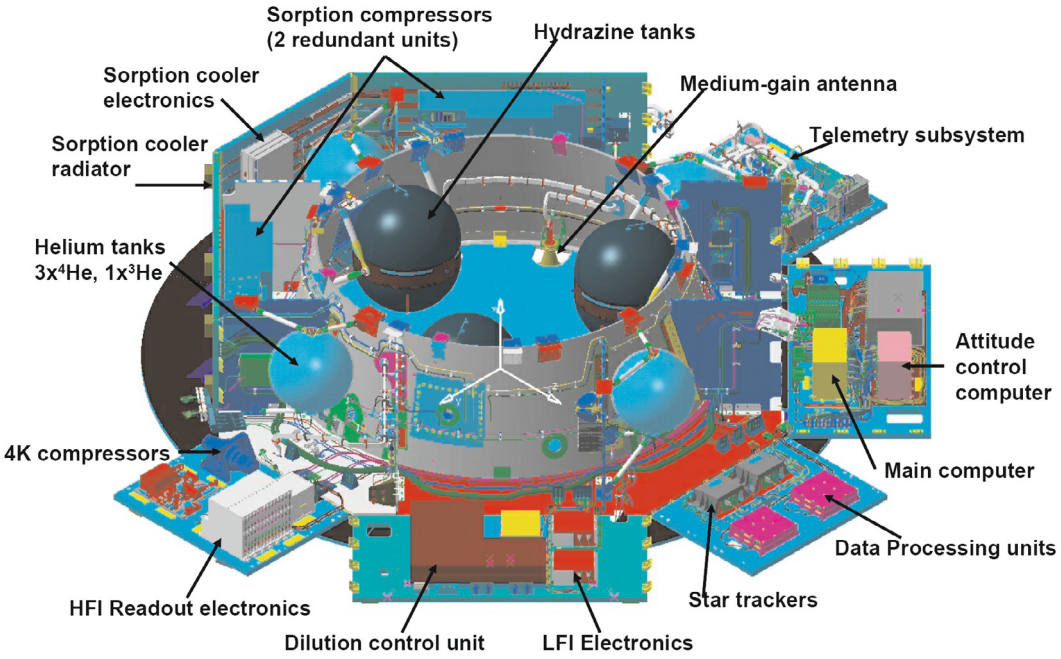

Fig. 6. The *Planck* service module consists of a conical mechanical structure around which is supported an octagonal set of panels. It contains all the warm satellite and payload electronic units, with the only exception of the box containing JFETs for impedance-matching to the HFI bolometers (see Fig. 5), which is mounted on the primary reflector support panel, to allow the operation of the JFETs at an optimal temperature of ~130 K . Figure courtesy of Thales Alenia Space (France).

values of $f_k \sim 20$ mHz, i.e. well below the required level which was set taking into account the satellite spin rate, $f_S \simeq 17$ mHz, and the efficiency of destriping algorithms (Maino et al. 2002; Keihänen et al. 2005).

2. *Radiometer thermal fluctuations* – The LFI front-end is cooled to 20 K for optimal sensitivity of the indium phosphide cryogenic amplifiers. Fluctuations in the temperature of the 20 K cold end lead to perturbations of the radiometric differential signal through a complex transfer function which depends on the thermal susceptibility of the active and passive components in the LFI front-end modules and on the damping properties of the instrument thermal mass (Mennella et al. 2010). Stability requirements imposed on the 20K sorption cooler (see Fig. 8) lead to fluctuations in the raw data of <10–15 μK (peak-to-peak), which translates into a residual systematic effect at a level <1 μK, estimated at the end of the mission after destriping. Similar requirements, though far less stringent, were imposed to the stability of the back-end modules where further RF amplification takes place.
3. *Thermal fluctuations of the reference loads* – Instabilities in the blackbody reference loads, connected to the HFI 4 K box, are directly transferred to the measured signals. Proportional-integral-derivative (PID) stabilisation applied to the HFI 4 K stage significantly reduces thermal fluctuations which are dominated by the 20 K pre-cooling interface. The effect has been calculated and eventually measured in the system level tests. The location of the PID on the 4 K stage leads to efficient damping for the 70 GHz reference loads (where an estimated level of the fluctuation spectrum below 10 $\mu K/\sqrt{\text{Hz}}$ is reached). The 30 and 44 GHz reference loads are located further away from the PID source, and for them a similar damping level is not guaranteed. On time scales below the spin rate (1 min), the thermal fluctuations of the reference loads are below the 10 $\mu K/\sqrt{\text{Hz}}$ requirement and do not contribute significantly to the noise in the differenced data. On longer time scales (~15 min), sorption cooler fluctuations on the HFI cold head induce periodic oscillations at the 4 K shield interface of order 5 mK (peak to peak) which propagate to the reference loads. The combination of the passive filtering due to the thermal inertia of the FPU itself and the action of the PID system completely suppress these oscillations in the 70 GHz loads, and reduce their amplitude to <1 mK in the 30 and 44 GHz loads. Simulations show that these fluctuations at low frequencies are efficiently erased by destriping techniques, leading to a residual effect on the maps of order 1 μK. Furthermore, the temperatures of the reference loads are measured by thermometers to an accuracy level which allows the removal of the thermal fluctuation signal, using software based on a thermo-mechanical model which has been specifically developed to deal with this effect if needed.
4. *Frequency spikes* – The noise spectra of some LFI radiometers exhibit a few very narrow spikes at 1 Hz and harmonics, which are known to be due to a subtle disturbance from the housekeeping data acquisition performed by the data acquisition electronics. These artifacts are nearly identical in sky and reference samples, and are almost completely removed by the LFI differencing scheme (Meinhold et al. 2009). Simulations reproducing the effect in a full-sky observation with worst-case assumptions lead to a residual systematic effect of 0.4 μK (peak-to-peak). Despite the extremely low level of this effect, software tools have been developed to remove the disturbance from the limited number of channels

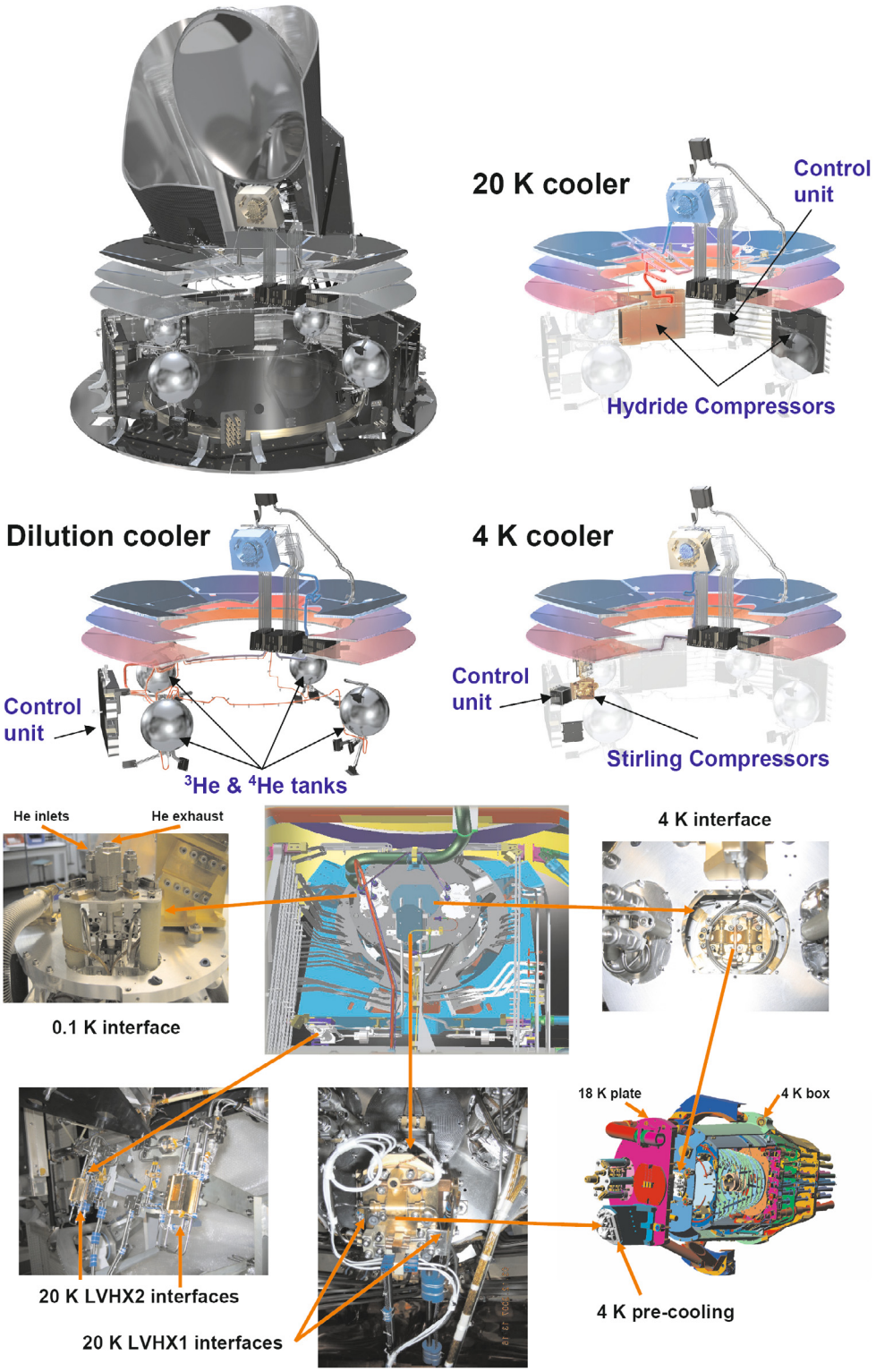

Fig. 7. The *top panel* of this figure shows the distribution of the elements of the three active coolers in various parts of the satellite. (*Top left*) The whole cooling system is closely integrated into the satellite. The three other panels at top show the elements of the 20 K sorption cooler, 4 K cooler, and 0.1 K cooler. Most of the cooler hardware is located in the Service Module; they all transport cryogenic fluids to the payload module via piping which is intricately heat sunk to the V-grooves. Details of the cooler connections to the focal plane can be seen in the composite shown in the lower part of the figure. Figures courtesy of ESA, LFI, and HFI.

showing it, and have been tested on the full *Planck* system-level tests, yielding a reduction factor of ∼10. Part of the comissioning phase of *Planck* will include careful in-orbit characterization of the spikes to further optimize the tools. Monte Carlo testing of the LFI analysis pipeline includes simulations and removal of these spikes.

Table 4. Summary of *Planck* instrument performance in flight, as predicted from ground characterisation (Mennella et al. 2010; Lamarre et al. 2010)

Instrument	LFI			HFI					
Center frequency [GHz]	30	44	70	100	143	217	353	545	857
Number of polarised detectors[a]	4	6	12	8	8	8	8		
Number of unpolarised detectors					4	4	4	4	4
Mean[b] FWHM (arcmin)	32.7	29.5	13.0	9.6	7.0	4.6	4.5	4.7	4.3
Mean[c] ellipticity	1.36	1.50	1.27	1.17	1.05	1.11	1.13	1.03	1.04
Bandwidth ($\Delta\nu$, GHz)	4.5	4.1	12	32	45	68	104	174	258
$\Delta T/T$ per pixel (Stokes I)[d]	3.3	5.2	8.9	3	2.2	4.8	2.0	150	6000
$\Delta T/T$ per pixel (Stokes Q &U)[e]	4.6	7.4	12.7	4.8	4.1	9	38		
Point source sensitivity[f] (1σ, mJy)	22	59	46	14	10	14	38	44	45

Notes. [(a)] For the LFI, the values shown correspond to the output of a linearly polarised differential radiometer; two such outputs, referred to as "detectors" in this paper, are supported by each horn. In fact each of the two radiometer outputs from one horn is built from the data acquired by two diodes, each of which are switched at high frequency between the sky and a blackbody load at 4 K (see Bersanelli et al. 2010). For the HFI, a (polarised) detector is taken to be the output of one of a pair of linearly polarised polarisation-sensitive bolometers; each horn contains one pair, i.e. two orthogonally-polarised detectors. Unpolarised spider-web bolometers are present in some of the horns, in these cases there is only one detector per horn. See Lamarre et al. (2010).
[(b)] Band-averaged, including polarised and unpolarised detectors, see Tauber et al. (2010).
[(c)] Band-averaged, including polarised and unpolarised detectors, see Tauber et al. (2010).
[(d)] In μK/K (thermodynamic temperature) for 15 months integration, 1σ, for square pixels whose sides are given in the row "Mean FWHM". The instantaneous sensitivities used for these estimates are drawn from ground calibration, averaged for all detectors in each channel; for LFI the sensitivity is the mean of the two methods described in Mennella et al. (2010).
[(e)] $\sqrt{2} \times \Delta T/T(I)$.
[(f)] Not including background confusion. Estimates of confusion levels can be extracted from Leach et al. (2008).

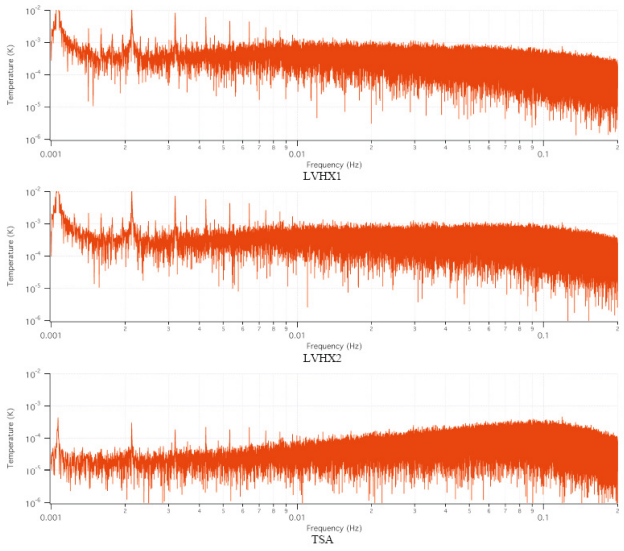

Fig. 8. Measured temperature fluctuation spectra at the two heat exchangers of the 20 K sorption cooler. LVHX1 is the interface to HFI which provides pre-cooling to the 4K cooler; the level of fluctuations seen by the HFI focal plane unit is damped significantly by the intervening mechanical structure, and further reduced by active control of the 4K plate. LVHX2 is the interface to the LFI focal plane; when the temperature control loop is used (TSA: *bottom panel*), the level of fluctuations is significantly reduced.

2.3.2. Deviations from ideality in HFI

The bolometers and readout system of HFI are intrinsically extremely stable (Lamarre et al. 2010), and the main instabilities that will affect the HFI are of thermal origin. Stability requirements on the temperature of the different HFI stages, throughout the frequency range where useful scientific data from the sky are sampled (0.016 to 100 Hz), are set by the following requirements (details can be found in Lamarre et al. 2010):

- by design, fluctuations in the 100 mK stage (carrying the bolometers) should induce an extra noise less than 20% of the background photon noise on the bolometers
- similarly, fluctuations in the 1.6 and 4 K stages (containing filters and horns in the optical path), should induce emission leading to stray-light levels less than 20% of the noise of the whole detection chain for all channels.

To achieve these stringent goals, each thermal stage within HFI is actively controlled:

- The temperature of the 4 K box, containing the back-to-back horns coupling to the sky, is regulated by a PID servo system with a heating belt providing a temperature stability such that the power spectrum of the temperature fluctuations is lower that 10 μK/ $\sqrt{\text{Hz}}$ within the band of sampling frequencies where useful information from the sky resides (0.016 to 100 Hz).
- A PID servo system controls the stability of the 1.6 K screen of the FPU (to which the bandpass-defining filters are attached) with a stability requirement of 28 μK/ $\sqrt{\text{Hz}}$ (in the range of frequencies 0.016 to 100 Hz).
- The bolometer temperature of 100 mK provides for very high sensitivity, limited mostly by the background photon noise, with a noise equivalent power around 10^{-17}W/ $\sqrt{\text{Hz}}$ for the channels near the peak of the CMB spectrum. The required temperature stability for this stage is thus very stringent: 20 nK/ $\sqrt{\text{Hz}}$ in the sampling frequency range 0.016 to 100 Hz. This is achieved mostly through a passive thermal filter mounted between the dilution cooler's cold tip and the bolometer optical plate. The mechanical link between these two stages is built out of a Holmium-Yttrium alloy which has a very high heat capacity in the 100 mK range, providing a thermal time constant of several hours between these stages.

In addition, two stages of PID regulation are included. The first is on the dilution cooler itself and it provides the long time stability. When no thermal perturbation is applied to the bolometer plate, this system provides the required stability. The stability at the lowest sampling frequencies (0.01 to 0.1 Hz) could be verified only marginally during system-level ground testing, because the thermal perturbations of the bolometer plate during the test were dominated by the dissipation of micro-vibrations due to the test tank environment. In the instrument-level tests, the heat input on the bolometer plate was around 10 nW with peaks at each filling of the liquid helium, creating drifts of a few μK over periods of a few hours. During the system-level tests the heat input from the facility was even larger (about 40 nW). The expected level in flight is less than 1 nW, caused by the bias current of the bolometer polarisation, and by Galactic cosmic rays deposited in the bolometer plate. The temperature fluctuations induced by these inputs should be negligible. The main temporary perturbations should instead come from solar flares: at most a few events are expected during the mission, which might lead to the loss of a few days of operations of the dilution cooler. A second PID temperature regulation is mounted on the bolometer plate itself but is only considered as a back up to the system described above and should not be needed in flight.

The instrument-level tests and system-level tests carried out have shown that the stability requirements are all satisfied (as described in detail in Lamarre et al. 2010; Pajot et al. 2010), although for the 100 mK stage the demonstration relies partly on analysis, as the level of micro-vibration of the test facilities did not allow to achieve flight-like thermal stability levels to be achieved (see Pajot et al. 2010), and therefore to measure reliable 1/f knee frequencies. The systematic effects due to temperature fluctuations are thus expected to be well below the noise and should not compromise the HFI sensitivity.

Additional systematic effects that are known to be significant for HFI include (more detailed descriptions are provided in Lamarre et al. 2010):

- *glitches* are due to cosmic rays entering the FPU through its metal box. The energy deposited in thermistors and radiation absorbers of bolometers are mostly above the noise and easily detected[5]. They will be detected and removed during preprocessing of the detector signal time lines by well-known software methods, e.g. Tristram (2005). During ground testing, the rate of glitches did not exceed a few per hour, but up to several per minute are expected in flight.
- Some channels suffer from a random bi-stable noise known in pre-amplifiers as *"telegraph" noise*. In all observed cases, the level of this noise did not exceed the standard deviation of the white noise component of the signal, i.e. 0.1 to 0.2 μvolts rms. The number of affected channels varied after every disconnection and reconnection of the low temperature harness. During the final tests at system level, after which the harness has not been manipulated, only the 143-8 and the 545-3 SWB channels showed a significant level of telegraph noise. Algorithms for removing this source of noise have been developed and have been tested on simulated signals. The residual extra noise will have to be evaluated in flight, but there is confidence that this phenomenon has limited consequences on the final noise at low frequencies.

[5] Lower energy cosmic rays and suprathermal particles from the solar wind do not reach the focal plane.

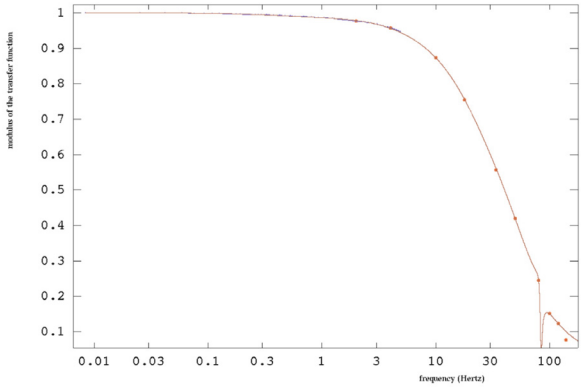

Fig. 9. The transfer function due to the time response of HFI bolometer 353-3a, as measured (blue and red dots) and modelled (red line).

- The compressors of the 4 K cooler induce strong *parasitic signals at the base frequency (~40 Hz) and harmonics*, through mechanical vibration and electrical interference on the low level part of the amplification chain. The microphonic component is suppressed to a negligible level by the design and active electronic vibration control system used to operate the 4 K cooler. The compressor cycle is phase-locked with the AC readout of the bolometers, which makes the parasitic lines of electromagnetic origin extremely narrow and easy to remove either in the time or the Fourier domain.
- Bolometers have thermal properties that induce a *non-instantaneous response* to incident radiation. In addition, their signal is processed by readout electronics which includes filters and an integration over several milliseconds of the digitized data. The resulting transfer function is complex (see Fig. 9), but in the domain of interest for scientific signals, it can be described as a first order low-pass filter with cut-off frequencies ranging from 15 Hz for the long wavelengths channels to 70 Hz for the short wavelength channels. In addition to this classical well-known behaviour, the HFI bolometers show an excess response at frequencies less than a few Hz, for which the amplitude of the response at very low frequencies is increased by a few per mil to a few per cent, depending on the channels. This excess response is well modelled by assuming that it originates from a parasitic heat capacity weakly linked with the bolometers. One consequence of this low frequency excess response is that the signal at 0.017 Hz from the CMB dipole, which is used for photometric calibration, will be enhanced at the percent level by this effect, while the response to higher order moments will not. In consequence, the transfer function has to be known and corrected to achieve an accurate measurement of the CMB spectrum. It has been measured on the ground with an accuracy better than 0.5% of the overall response. The measurement will be repeated in orbit by injecting electrical signals in the bolometers. The signal from planets and from the Galaxy will provide additional constraints on this parameter. More details can be found in Lamarre et al. (2010).

2.4. Optics

A detailed description of the *Planck* telescope and the instrument optics is provided in Tauber et al. (2010), Sandri et al. (2010) and Maffei et al. (2010). The LFI horns are situated in a ring around the HFI, see Fig. 4. Each horn collects radiation from the telescope and feeds it to one or two detectors. As shown in Fig. 4 and Table 4, there are nine frequency bands, with central frequencies varying from 30 to 857 GHz. The lowest

three frequency channels are covered by the LFI, and the highest six by HFI. All the detector optics are mono-mode, except for the two highest frequencies which are multi-moded. The mean optical properties at each frequency are given in Table 4, as derived from ground measurements in combination with models extrapolating to flight conditions.

The arrangement of the detectors in the focal plane is designed to allow the measurement of polarisation parameters Stokes Q and U (see e.g. Couchot et al. 1999). Most horns contain two linearly polarised detectors whose principal planes of polarisation are very close to 90° apart on the sky. Two such horns, rotated by 45° with respect to each other, are placed consecutively along the path swept by the field-of-view (FOV) on the sky. This arrangement enables the measurement of the Stokes Q and U parameters by suitable addition and subtraction of the different detector outputs, and reduces spurious polarisation due to beam mismatches.

Uncertainties in the beam shape have a direct impact on the calibration of the temperature scale, which increases with decreasing angular scale. The knowledge of the beams achieved on the ground (Tauber et al. 2010) is close to, but not enough to achieve the calibration accuracy goals (1% at all multipoles up to 2000 in the 70–217 GHz frequency channels, and 3% at other frequencies). It will be supplemented with measurements of planets during flight (see Sect. 4.2).

Each linearly polarised detector is mainly (but not only) characterised by two parameters: the orientation on the sky of the principal plane of polarisation, and the cross-polar level (i.e. the sensitivity to radiation polarised orthogonally to the principal plane). Both these parameters have been measured on the ground, with accuracies described in Leahy et al. (2010) and Rosset et al. (2010); a summary for both instruments is provided in Tauber et al. 2010. These measurements will be complemented in flight with observations of a bright and strongly polarised source, the Crab Nebula (Tau A). This compact source has well-known polarisation characteristics whose knowledge is now being improved specifically for *Planck* (Aumont et al. 2010). The details of the polarisation measurement and calibration scheme are developed further in Leahy et al. (2010) and Rosset et al. (2010).

Other systematic effects related to the optics (described in greater detail by Tauber et al. 2010) include:

- stray-light originating in the CMB dipole is slowly varying and will be very effectively removed by data processing, e.g. destriping.
- stray-light originating from Galactic emission results in a significant signal level for temperature anisotropies, the main features of which have been extensively studied, and can be effectively detected and removed (Burigana et al. 2006). The level of polarised stray-light is much more difficult to predict but should also be at a controllable level (Hamaker & Leahy 2004).
- stray-light originating from solar system bodies is expected to be insignificant
- fluctuating self-emission from satellite surfaces, mainly the telescope surfaces, is at a very low level and can be identified with the help of on-board thermometry.

2.5. On-board data acquisition, handling and transmission to ground

Data are acquired continuously by both instruments and delivered to a central solid-state memory, from which it is downlinked to ground during a daily contact period of 3 h at a rate of 1.5 Mbps via a medium-gain antenna which may be used within a ±15° Earth cone (see Fig. 2). The effective total real-time acquisition rate allocated to the two instruments is 130 kbps averaged over a full day (53.5 kbps allocated to LFI and 76.5 kbps to HFI). The minimum data sampling frequency of the *Planck* detectors is determined by the need to fully sample all beams in the along-scan direction. Using as guideline the 1-D Nyquist criterion, the beams should be sampled at least 2.3 times per $FWHM$. In the cross-scan direction, this is ensured by the manoeuver step size of 2 arcmin (Sect. 3.3). Along the scan circle, the readout electronics, digitisation and on-board processing provide the required sampling as described below.

The data handling scheme for LFI is described in detail in Maris et al. (2009). For each detector, LFI samples both sky and reference load signals from each detector at ~8.2 kHz, and then averages the samples down to 3 bins per beam $FWHM$. The analog-to-digital noise added in the process is negligible. The sky and reference load time-ordered data are then "mixed" to reduce variability due to correlated noise and drifts, and re-quantised to an equivalent[6] $\sigma/q \sim 9$, leading to a $\sigma/q \sim 2$ for the sky and reference recovered signals. This process adds less than 0.05% extra white noise (see Maris et al. 2004 for a description of the effects of quantisation on the noise distribution). Finally, the mixed and re-quantised time-ordered data are recoded using an adaptive lossless algorithm into packets of maximum capacity of 980 bytes equivalent to about 1172 compressed samples. Each packet is coded in such a way that decoding does not depend on any other packet. The on-board process is complicated but allows the recovery on the ground of both sky and reference load time-ordered data with negligible added noise. The average data rate for all LFI detectors resulting from this process is ~49 kbps (including housekeeping telemetry).

The HFI scheme is based on sampling all detectors at a constant frequency of 180 Hz, which results in a beam sampling rate which varies from 2.2 at the 4 highest frequency channels, to 4.8 at 100 GHz. The samples are then quantised to $\sigma/q \sim 2$, which adds an excess white noise of ~1%. After lossless compression into packets of 254 consecutive samples, using an algorithm similar to that of LFI, the average data rate of all HFI detectors is ~68 kbps (including housekeeping telemetry).

The total science data volume downlinked each day is thus ~13 Gbit. The on-board memory has capacity to store at least 2 days of data in case one contact period is missed.

Time stamping of LFI and HFI data acquisition is synchronised to a central on-board clock with a precision of 15 μs; the synchronization of star tracker data is also based on the central clock so that the relative accuracy of sample location on the sky is extremely good. The on-board clock itself can be synchronised to ground (e.g. UT) during the ground visibility periods with high precision. Ground tests show that drifts during the non-visibility period are mostly correlated with thermal fluctuations and at a level below 0.1 μs per day.

2.6. Lifetime

The required lifetime of *Planck* in routine operations (i.e., excluding transfer to orbit, commissioning and performance verification phases which span ~3 months in total) is 15 months, allowing it to complete two full surveys of the sky within that

[6] σ is the rms of the samples being compressed, whereas q is the amplitude of the least significant bit in each compressed word. The value of q is set by telecommand only when needed to keep the total daily data volume of LFI within the allocated value.

Fig. 10. An artist's impression of *Herschel* and *Planck* in launch configuration, under the fairing of the Ariane 5 rocket. *Planck* is attached to the rocket interface by means of a ring-shaped clampband. A cylindrical structure surrounds *Planck* and supports *Herschel*. Figure courtesy of ESA (C. Carreau).

period. Its total lifetime is limited by the active coolers (see Sect. 3) required to operate the *Planck* detectors. In particular:

- the dilution cooler, which cools the *Planck* bolometers to 0.1 K, uses ^{3}He and ^{4}He gas which is stored in tanks and vented to space after the dilution process. System-level tests of the *Planck* satellite have verified that the tanks carry enough gas to provide an additional lifetime of between 11 and 15 months over the nominal lifetime, depending on the exact operating conditions found in flight.
- the lifetime of the hydrogen sorption refrigerator, which cools the *Planck* radiometers to 20 K and provides a first precooling stage for the bolometer system, is limited by gradual degradation of the sorbent material. Two units fly on *Planck*: the first will allow completion of the nominal mission; the second will allow an additional 14 months of operation. A further increase of lifetime could be obtained, if needed, by heating the absorbing material to a high temperature (a process known as "regeneration").

Overall, the cooling system lifetime will probably allow at least one additional year of operation beyond the current nominal mission span. Barring failures after launch, no other spacecraft or payload factors impose additional limitations. An additional year

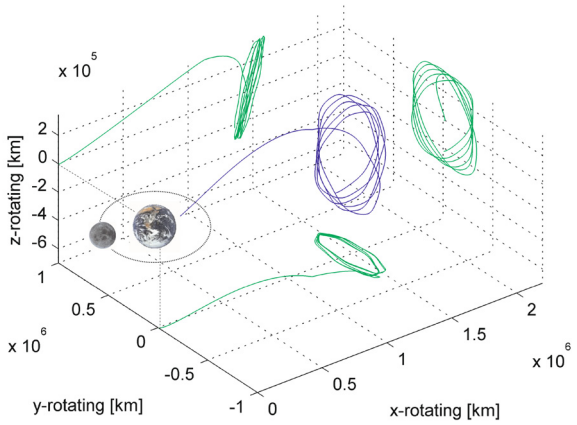

Fig. 11. The trajectory which transfers *Planck* from rocket release to its final orbit around the L2 point, in Earth centered coordinates. Five orbits around L2 are sketched. The orbital periodicity is ~6 months. The lunar orbit is indicated for reference; the Earth and Moon are not to scale. Figure courtesy of ESA (M. Hechler).

of lifetime increase would allow *Planck* to complete four full surveys of the sky instead of the nominal two surveys.

Such an extension of the *Planck* mission would provide improved calibration, control of systematic errors, and noise, leading to reduced uncertainties for many of *Planck*'s science goals and legacy surveys. These improvements will be particularly important for *Planck*'s polarisation products, for which noise, systematic errors, and foregrounds are all potentially limiting factors.

3. Operational plans

3.1. Launch, transfer, and final orbit

Planck was launched from the Centre Spatial Guyanais in Kourou (French Guyana) on 14 May 2009 at 13:12 UT, on an Ariane 5 ECA rocket of Arianespace[7]. ESA's *Herschel* Space Telescope was launched on the same rocket, see Fig. 10. Approximately 26 min after launch, *Herschel* was released from the rocket at an altitude about 1200 km above Earth, and *Planck* followed suit 2.5 min later. The Ariane rocket placed *Planck* with excellent accuracy on a trajectory towards the 2nd Lagrangian point of the Earth-Sun system ("L2") which is sketched in Fig. 11[8]. The orbit describes a Lissajous trajectory around L2 with 6 month period that avoids crossing the Earth penumbra for at least 5 years.

After release from the rocket, three major manoeuvers were carried out to place *Planck* in its intended final orbit: the first, intended to correct for errors in the rocket injection, was executed within 2 days of launch; the second at mid-course to L2; and the third and major one to inject *Planck* into its final orbit. These manoeuvers took place on 9 June and 3 July, and they were carried out using *Planck*'s coarse (20 N) thrusters. Once in its final orbit, very small manoeuvers are required at approximately monthly intervals to keep *Planck* from drifting away from its intended path around L2.

Once in its final orbit, *Planck* will survey the sky continuously for a minimum of 15 months, allowing to survey the full

[7] More information on the launch facility and the launcher is available at http://www.arianespace.com

[8] The final orbit of *Herschel* around L2 is much larger than that of *Planck*, 900 000 km vs. 400 000 km maximum distance to the Earth-L2 line. Their transfer trajectories are therefore quite different.

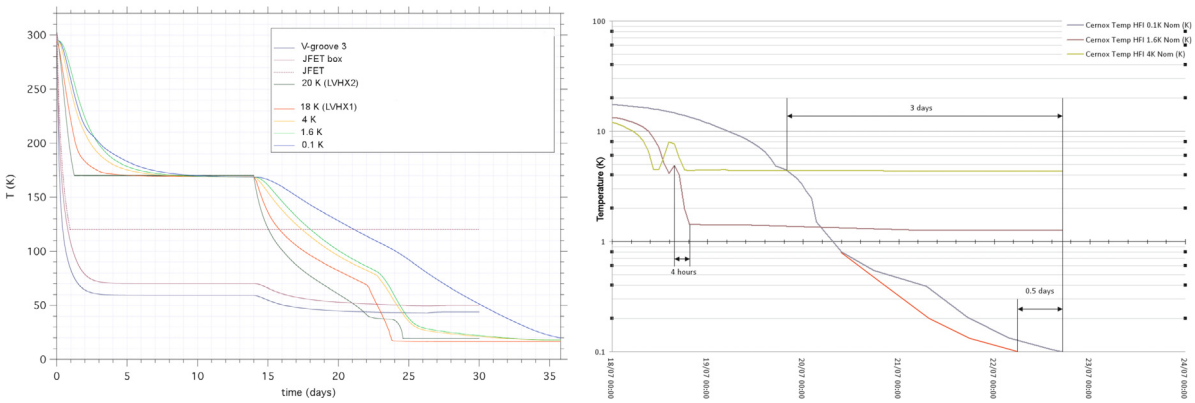

Fig. 12. *The left panel* shows the predicted initial cool-down profiles of the temperature stages in the coolers. The plateau at 170 K is created by heating, to prevent outgassing from contaminating the reflector and focal plane sufaces. The model does not represent the cool-down profiles of the actively cooled stages accurately: *the right panel* shows the profile measured during on-ground tests, which is expected to be close to the in-flight profile. Figures courtesy of HFI (J.-L. Puget).

sky at least twice. It will operate autonomously, driven from an on-board timeline which is uploaded daily during the 3 h period of contact with the ground. The contact period will also be used to downlink to ground the data which have been acquired over the past 24 h.

3.2. Payload commissioning and performance verification

Functional commissioning started immediately after launch, first addressing critical satellite subsystems, and secondly the payload. At the time this paper is being submitted for publication, the commissioning activities are completed, and all on-board systems are behaving nominally.

Initially, the telescope reflectors and the focal plane were heated to prevent contamination by outgassing from other payload elements. As soon as heating was removed (about two weeks after launch), the payload cooled radiatively rather quickly, see Fig. 12. During this phase, the cryo-chain was gradually turned on and commissioned. The temperature profile achieved during cool-down was also used to tune and evaluate the LFI's radiometric performance. The coldest temperature of 0.1 K was reached about 50 days after launch. At this time a one month phase of activities started, dedicated to the optimisation of the settings of the cryo-chain and the two instruments. This phase culminated with a two-week period of observations mimicking routine surveying, after which small adjustments to the settings could have been made (but were not necessary), before the start of the survey phase.

3.3. Surveying strategy

After the initial commissioning and performance verification phases were completed, *Planck* started to survey the sky and was scheduled to do so during 15 months[9]. No interruptions or alterations in the scanning strategy need to be made for polarisation calibration or beam mapping, since the corresponding sources will anyway be observed. During this period the satellite moves in its orbit around L2 and L2 around the Sun. Its spin axis is actively displaced on the average 1° per day in ecliptic longitude to maintain its anti-Sun direction (see Fig. 13). The instrument Field-of-View rotates around the spin axis and will cover the full sky at least twice over within the nominal survey period.

[9] The satellite carries enough cryogens to allow an extra 12 months of operation.

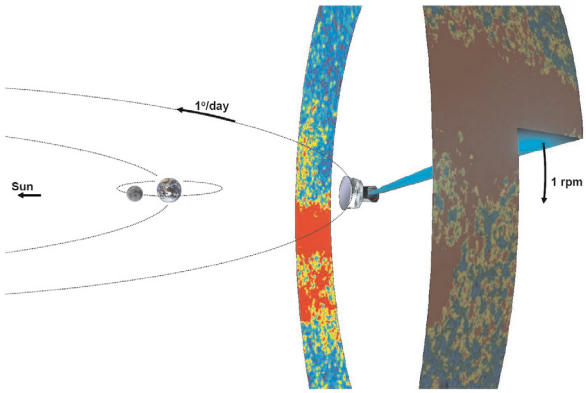

Fig. 13. From its orbit around L2 (Fig. 11), *Planck* will scan the sky as its Field-of-View rotates at 1 rpm. The spin axis is moved on average by 1°/day (in 2 arcmin steps) to maintain the spin axis at a constant aspect angle to the Sun of 7.5°.

Table 5. Scanning strategy parameters.

θ	7.5
ω	2π/(6 months)
ϕ	340°
n	1
Step	2 arcmin

General considerations on the exact choice of the path to be followed by the spin axis are described in Dupac & Tauber (2005) and Delabrouille et al. (2000). The cycloidal spin axis path selected allows *Planck* to maintain a constant aspect angle to the Sun and to cover the whole sky with each detector in the FOV. It is defined by the following functions[10]:

$$\lambda = \theta \sin[(-1)^n \omega(t - t_0) + \phi] \quad (2)$$

$$\beta = -\theta \cos[(-1)^n \omega(t - t_0) + \phi] \quad (3)$$

where λ is the angular distance from the fiducial point in Ecliptic longitude, β the angular distance from the fiducial point (the anti-Sun direction) in Ecliptic latitude, θ the spin axis precession

[10] These equations are not exactly followed by the mission planning software, which corrects for the variation of the Earth's orbital speed on the path of the cycloid, but the differences are small enough to be negligible for the purpose of characterising the survey coverage.

amplitude, ω the pulsation of the precession, ϕ its phase, n the parameter which controls the motion direction of the precession, t is the time, and t_0 is the first time during the *Planck* survey at which the fiducial point crosses the 0° Ecliptic longitude line. The values of these parameters are – with the exception of n and ϕ – independent of the launch date (see Table 5). The choice of n and ϕ is made based on a tradeoff of the following criteria related to detector calibration:

- Allowing the largest possible difference between two successive sky surveys of the scan angle on the Crab, to improve the calibration of polarisation properties. The maximum possible difference is 15° (determined by the Earth angle constraint). The selected scanning parameters result in an angle difference of ∼13.°5.
- Avoiding satellite orientations which would lead to very low amplitudes of the CMB dipole during parts of the survey, to improve the photometric calibration.
- Ensuring that when the brightest planets are observed (for beam calibration), there is sufficient operational margin to reobserve them in case of need.

The motion of the spin axis along its cycloidal path is not continuous, but achieved by manoeuvers whose amplitude is fixed to 2 arcmin. This step size has been set to ensure adequate sampling of even the smallest beams in the cross-scan direction. Between manoeuvers (whose typical duration is 5 min), the satellite spin axis is inertially stable, except for residual nutation and a drift due to solar pressure (estimated at 2.5–3.5 arcmin/day). As a consequence of the fixed size step manoeuvers and the orbital characteristics, the inertial dwell times vary sinusoidally with 6 month period between 2360 and 3904 s.

With this scanning strategy, and assuming no interruptions, the typical sky coverage that will be achieved is illustrated in Figs. 14 and 15, and quantified in Table 6 for representative frequencies. The range of coverage parameters found depends largely on the size of the circle; the difference between the 30 and 44 GHz horns being the largest as they are located at two extremes of the focal plane.

Table 6. Sky coverage (15 months survey, average per frequency).

Frequency (GHz)	Mean[a] (s/sq. deg.)	Low[b] (%)	High[c] (%)	Deep[d] (%)	Pol. Stat.[e] (%)
30	953	4.5	1.7	0.42	0.8
44	953	3.3	1.5	0.28	3.7
100	953	4.3	1.5	0.41	0.61
353	953	4.3	1.2	0.37	0.10

Notes. [(a)] Integration time per square degree for typical channels. [(b)] Fraction of the sky with integration time lower than one-half the mean value. [(c)] Fraction of the sky with integration time higher than four times the mean value. [(d)] Fraction of the sky with integration time higher than nine times the mean value. [(e)] Fraction of the sky which has a high spread of scanning angles, for all detectors at each frequency. The value is based on dividing the 2π range of angles into 16 bins; for a pixel on the sky, the spread is considered high if there are samples in at least 5 bins. More details are available in Dupac & Tauber (2005).

4. Calibration strategy

The calibration – conversion of raw data to physical units – requires specific measurements to be made, some of which can only be made on the ground, and some of which will be primarily, or at least partially, obtained in flight.

4.1. On-ground calibrations

The calibration campaigns carried out on the ground and their results are described in detail in Pajot et al. (2010) (HFI), Mennella et al. (2010) (LFI), and Tauber et al. (2010) (Telescope). The results of these campaigns form a complete calibration set which is the basis for the performance estimates made in this paper. Some parts will be superseded by measurements in flight, but others cannot be improved in flight (though some may be verified in flight). The latter group includes:

1. The spectral response of each detector, the knowledge of which is described in Villa et al. (2010) (LFI) and Ade et al. (2010) (HFI).
2. The linearity of each detector, the knowledge of which is described in Villa et al. (2010) (LFI) and Pajot et al. (2010) (HFI).
3. Cross-correlations between detectors, which can be verified in flight using the brightest planets. Upper limits determined on the ground are described in Mennella et al. (2010) (LFI) and Pajot et al. (2010) (HFI).
4. Thermal susceptibilities of the detectors, i.e. their response to variations in the thermal environment, the knowledge of which is described in Mennella et al. (2010) (LFI) and Pajot et al. (2010) (HFI).

4.2. In-flight calibrations

In-flight calibrations are based on the observation of four distinct classes of sources:

- the so-called "CMB dipole", i.e. the modulation of the CMB due to the motion of the solar system barycenter with respect to the cosmological comoving frame, has an amplitude of ∼3.4 mK which is known to an accuracy of ∼0.3% (Hinshaw et al. 2009); it is further modulated by the motion of the Earth around the Sun, with an amplitude (∼10% of the dipole itself) which can be very accurately calculated from the orbital velocity of the satellite with respect to the Earth (which can be estimated in flight with an accuracy better than 1 cm/s), and that of the Earth around the Sun (which is extremely accurately known). These variations are visible in the *Planck* time-ordered data at periods of one minute and 6 months respectively, and are sufficient to calibrate the responsivity to large-scale CMB emission of all *Planck* detectors up to 353 GHz with an accuracy better than 1% (see Bersanelli et al. 1997; Cappellini et al. 2003, for LFI, Piat et al. 2002, for HFI).
- at the highest frequencies of HFI, namely 545 and 857 GHz, the CMB dipole signal is too faint to be a good photometric calibrator. Instead the ∼7° resolution maps obtained by the Far-Infrared Absolute Spectrometer (FIRAS) instrument on board COBE of emission from the Galactic Plane will be used as a calibrator. Detailed simulations which take into account various significant effects, i.e. the precision of COBE/FIRAS measurements, the emission spectrum of the Galactic Plane and its knowledge, the stability of the HFI detectors over one week period (needed to sweep over the extent of the FIRAS resolution) and the ability to monitor this stability using celestial sources, leads to an expected absolute accuracy better than ∼3% (Piat et al. 2002).
- Observations of bright planets (in effect the brightest point sources in the *Planck* sky) will be used (as outlined in

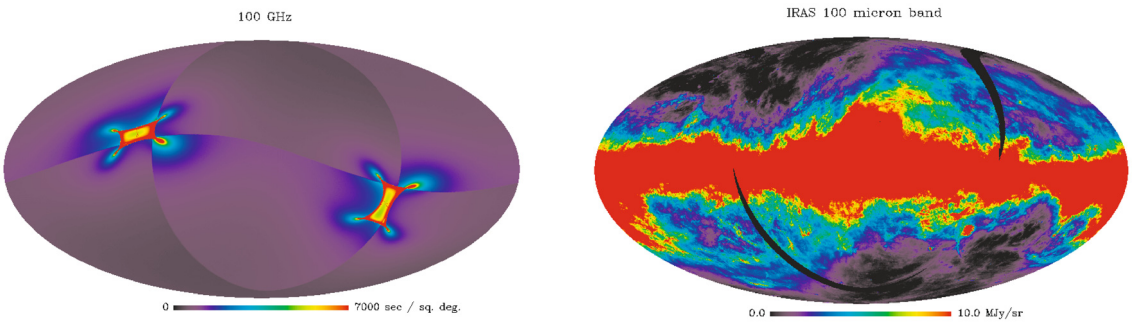

Fig. 14. *Left panel*: coverage map achieved after 15 months of survey at 100 GHz, in units of integration time (blue to red color scale corresponds to 350 to 7000 s/deg^2.). The map is a Mollweide projection of the whole sky in Galactic coordinates, pixelised according to the Healpix (Górski et al. 2005) scheme at Nside = 1024. This map is typical of the coverage at all frequencies; the shape of the high-integration regions around the ecliptic poles changes slightly with frequency, as illustrated in Fig. 15. For comparison, in the right panel is shown a map of IRAS 100 μm emission, showing the typical extent of Galactic dust emission; it also shows that the *Planck* "deep fields" are not the cleanest in terms of diffuse Galactic emission. Figures courtesy of ESA (X. Dupac).

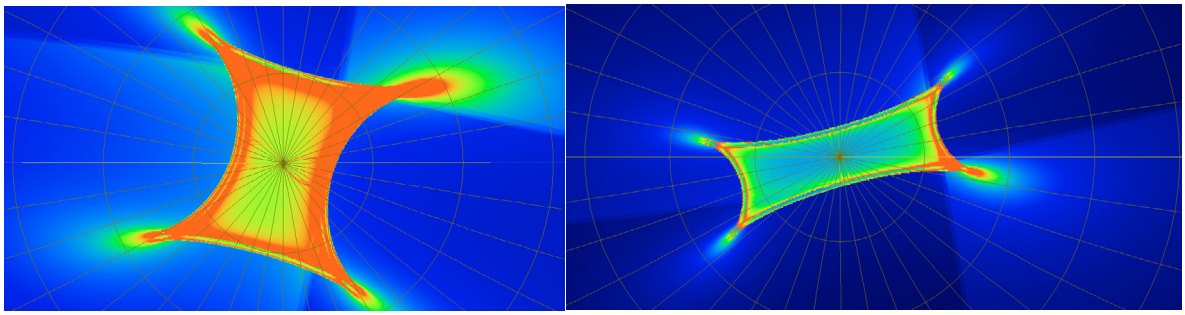

Fig. 15. Coverage map near the North ecliptic pole, achieved after 15 months of survey at 70 GHz (*left*) and 217 GHz (*right*), in units of integration time (blue to red color scale corresponds to 378/356 to 15 000 s/deg^2 for 70/217 GHz respectively). The horizontal extent of the maps is 63° at 70 GHz and 72° at 217 GHz (the angular separation between radial lines from the ecliptic pole is 10°). The figure illustrates how the shape of the highest integration areas narrows and rotates with frequency. Figures courtesy of ESA (X. Dupac).

Tauber et al. 2010 and described in detail most recently in Huffenberger et al. 2010) to:

- map the angular response of each detector. For this purpose Jupiter and Mars are especially important. In the worst case analysed, using no information about the optics except the measurement of planets, Huffenberger et al. (2010) find that a single transit of Jupiter across the focal plane will measure the beam transfer functions to better than 0.3% for the channels at 100–217 GHz which are the most sensitive to the CMB.
- determine the focal plane geometry, i.e. the relative location of all detectors on the sky.
- Determine the time response (long-timescale component) of the HFI detectors.

The planets will be observed without any interruption or indeed modification of the routine scanning strategy; about one week of time is needed to scan the full FOV across a planet. Each planet is encountered at least once in each full sky survey; successive observations will be used to improve the determination of the above parameters and assess any possible long-term drifts.

- Bright polarised point sources (mainly Taurus A – the Crab) will be used to determine the absolute orientation of the principal angle of polarisation and the cross-polarisation level of each *Planck* detector. The relative angle can be determined by observation of regions of brightly polarised foreground emission at high ecliptic latitudes (which are observed many times with a wide range of scan angles). Some further details of the calibration scheme and its accuracy are described in Tauber et al. (2010) and Leahy et al. (2010).

The *Planck* thermal model will be used to predict temperatures and thermal fluctuation levels at all critical locations in the focal plane (e.g. detectors, filters, reference loads, etc) based on the available on-board thermometry, and is a required element of the calibration process. It consists of two distinct models: one addressing the large-scale quasi-static heat flows, which is used mainly for cool-down and warm-up predictions; and one which models the actively cooled elements. Both have been correlated extensively with ground measurements, and modified accordingly. Since the ground test environments can never fully mimic the flight situation, these models will be re-correlated during the early phases of operations, and a publication describing the results will be produced at that time.

5. The "scientific ground segment"

The ground operations of the *Planck* satellite are based on 4 geographically distributed centres (see Fig. 16):

- The mission operations centre (MOC), located at ESA's operations centre in Darmstadt (Germany), is responsible for all aspects of flight control and of the health and safety of the *Planck* satellite, including both instruments. It plans and executes all necessary satellite activities, including instrument commanding requests by the instrument operations centres. MOC communicates with the satellite using ESA's 35-m antenna located in New Norcia (Australia) over a daily 3-h period, during which it uplinks a scheduled activity timeline which is autonomously executed by the satellite, and downlinks the science and housekeeping (HK) data acquired by

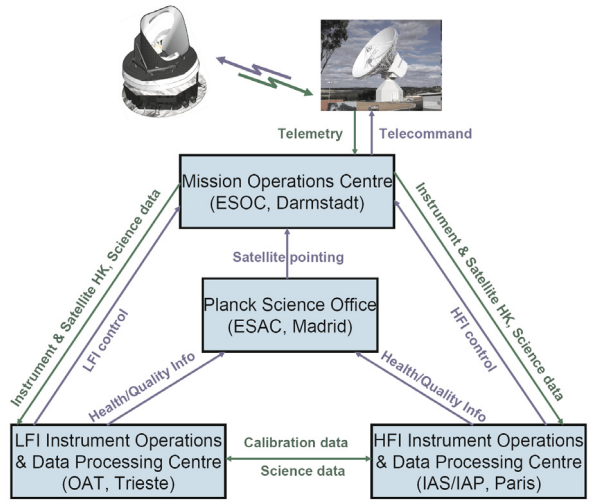

Fig. 16. A sketch of the centres involved in the *Planck* ground segment and the main data exchanges between them.

the satellite during the past 24 h. The downlinked data are transferred from New Norcia to the MOC over a period of typically 8 h; at MOC they are put onto a data server from where they are retrieved by the two Data Processing Centres.

– The *Planck* Science Office (PSO), located at ESA's European Space Astronomy Centre in Madrid (Spain) is responsible for coordinating scientific operations of the *Planck* instruments, and for planning the sky surveying strategy. It provides to MOC a detailed pointing plan with a periodicity of about 1 month. PSO will also develop and operate the archive which will store and distribute the final scientific products to the community.
– The LFI instrument operations and data processing centre, located at the Osservatorio Astronomico di Trieste (Italy), is responsible for the optimal operation of the LFI instrument, and for the processing of the data acquired by LFI into the final scientific products of the mission.
– The HFI instrument operations and data processing centres, located respectively at the Institut d'Astrophysique Spatiale in Orsay (France) and at the Institut d'Astrophysique de Paris (France), are similarly responsible for the optimal operation of the HFI instrument, and (with several other institutes in France and the UK) for the processing of the data acquired by HFI into the final scientific products of the mission.

The principal objective of *Planck* is to enable CMB-based scientific analysis, as described in the Planck Bluebook. The success of the mission depends on the combination of measurements from both instruments to produce a sensitive and well-understood set of maps of the Stokes I, Q and U components of the CMB anisotropies . The combination of LFI and HFI data poses significant challenges arising from the different technologies involved, but also provides advantages in terms of cross-checking and cross-calibration. To use these advantages fully requires the co-analysis of LFI and HFI data at all levels starting at that of individual detector timelines, and not only at the level of frequency channel maps. The two data processing centres (DPCs) have set up a system of periodic data exchanges which is geared to make full use of these advantages and to ensure that a single coherent set of products is generated by the mission. The philosophy underlying this system is that:

– The calibration of each instrument and cleaning of spurious artifacts requires deep expert knowledge and is carried out within each DPC; nonetheless, LFI and HFI data (timelines, detector maps, frequency channel maps) are exchanged at frequent intervals to allow cross-calibration and cross-checking for systematic effects as much as possible.
– Frequency maps will be produced by each DPC for their respective instruments and will form a common input to component separation pipelines which are geared to isolate the CMB signals from all systematic effects and non-CMB signals (so-called "foregrounds"). Finding the best algorithm for this purpose will be an iterative process involving both DPCs.
– Scientific analysis is the main driver in the search for the best products and cannot be separated from data calibration or processing issues; it is therefore intertwined and will also be repeatedly iterated. To enable this feedback to take place, the DPCs will issue at regular intervals (typically 6 months) products - principally maps – of increasing sophistication and quality for the scientific users within the *Planck* Collaboration (see Annex 1).

The iterative data processing outlined above will gradually yield a mature set of scientific products which will be delivered by the DPCs to ESA 2 years after the end of the baseline surveying period of 15 months[11]. The data products, which will be distributed to the community via an online archive developed by ESA about 3.5 years after launch (i.e. in November 2012), will consist of:

– Calibrated and cleaned time-ordered data for each detector.
– Maps of the whole sky at each *Planck* frequency. This is the main product of the mission.
– All-sky Stokes *I, Q,* and *U* maps of the CMB anisotropies
– All-sky Stokes *I, Q,* and *U* maps of a set of non-CMB components, the exact definition of which is still open, but which will contain at least Galactic synchrotron, free-free, and dust emission; and most likely also the diffuse (unresolved) Sunyaev-Zeldovich and extragalactic background.
– An all-sky catalogue of compact and point sources extracted from the *Planck* sky maps. These sources will include both Galactic and extra-galactic sources. Of particular interest among the extra-galactic sources will be those detected via the signature of the Sunyaev-Zeldovich effect.
– A sufficient set of information and data which allows the products to be useable by a typical astronomer, e.g. calibration data, uncertainty descriptors, likelihood functions, ancillary data used in the product generation, descriptive documentation, etc.

In addition to the above products, an Early Release Compact Source Catalogue (ERCSC) will be released to the community ~19 months after launch, which is targeted to identification and quick follow-up of scientifically interesting objects, in particular by the limited-lifetime *Herschel* Observatory[12]. The ERCSC will be based on the data gathered during the first sky survey only, and the detection algorithm will emphasize reliability of the included sources rather than completeness. The algorithm will not attempt to use any channel cross-correlation information, except in the case of two particular classes of sources which are of particular interest for *Herschel* follow-up and which will be identified on specific color criteria, namely Galactic cold cores and extragalactic Sunyaev-Zeldovich sources. The typical

[11] If the *Planck* mission is extended by a year, the first delivery of products based on the initial period will be followed by a second delivery, one year later, of products based on the full data set.
[12] See http://www.esa.int/Herschel

flux limit of the ERCSC at high Galactic latitudes will be $\sim 10\sigma$ of the noise or confusion level (see Table 4).

6. The core scientific programme

The organisation of the *Planck* Collaboration (see Appendix A) is geared not only to generate the final scientific products described in Sect. 5, but also to enable scientific analysis during the proprietary period. The science potential of *Planck* has been described previously in detail in the Planck Bluebook. The *Planck* Collaboration is focussing its efforts into a number of areas each covering a set of well defined projects (as enumerated below). Each of the projects has been assigned to a specific team of people within the overall Collaboration. In most cases a substantial amount of preparatory work has been done by these teams so that scientific papers can be completed by the time that the products of *Planck* are publicly released. Together, these projects form the core of the *Planck* Scientific Programme:

1. **CMB-based cosmology**
   (a) Analysis of the isotropy and statistics of the CMB anisotropies, in particular by
      – blind application of a range of statistical tools to the CMB maps;
      – investigation of the large-scale "anomalies" suspected in the WMAP data;
      – investigation of large-scale "anomalies" in *Planck* polarization maps.
   (b) Estimation of the temperature and polarisation angular power spectra and likelihood functions
   (c) Estimation of cosmological parameters, based on
      – *Planck* data alone
      – *Planck* data and constraints from other astrophysical data. Special attention will be paid to constraints which can be put on inflationary models.
   (d) Search for and constraints on B-mode polarisation anisotropies.
   (e) Determination of the gravitational lensing signatures in the CMB caused by intervening large-scale structure.
2. **Non-Gaussianity of the CMB**
   (a) Bispectrum analysis and constraints on the $f_{\rm NL}$ parameter for "squeezed" triangular wave vector shapes and of more general forms of non-Gaussianity.
   (b) Testing any measured non-Gaussianity against the predictions of specific inflationary models (e.g. multi-field inflation, curvaton perturbations, DBI inflation etc.).
   (c) Measuring or setting upper limits on the existence and strength of primordial magnetic fields.
   (d) Probing the geometry and topology of the Universe, by testing against the predictions of specific models such as Bianchi universes.
   (e) Testing for the presence of cosmic strings or other classes of defects.
3. **Secondary anisotropies**
   (a) Production and analysis of a catalogue of Sunyaev-Zeldovich (SZ) sources detected by *Planck*.
   (b) Analysis of the combination of *Planck* SZ-selected galaxy clusters with a wide range of other observations (X-ray, optical, near-IR, sub-mm), either from existing surveys or by dedicated follow-up, to study their physics and evolution.
   (c) Reconstruction of the ionisation history of the Universe.
   (d) Estimation of the Integrated Sachs-Wolfe effect and its constraints on cosmological parameters e.g. the dark energy equation of state.
   (e) Extraction and analysis of diffuse and kinetic Sunyaev-Zeldovich components.
4. **Extragalactic sources**
   (a) Analysis of the statistical properties and evolution of radio and sub-mm sources, and their classification into dominant populations
   (b) Survey of extreme radio sources, i.e. those with unusual, sharply peaked, or inverted spectra.
   (c) Construction and analysis of a catalogue of quasars and BL Lac objects, combining *Planck* data with data from a wide variety of other wavelengths. Specific effort is being made to detect flaring sources and follow them up quickly with ground facilities.
   (d) Construction and analysis of a catalogue of nearby galaxies, and the detailed study of a small number of resolved galaxies (LMC, SMC, M 31, M 33).
   (e) All-sky survey and analysis of bright high-redshift dusty galaxies, and possibly proto-clusters.
   (f) Extraction of the cosmic far-infrared background believed to consist of unresolved galaxies, and analysis of the angular power spectra of this component.
5. **Galactic science**
   (a) Construction of a model of the large scale ordered magnetic field in the Galaxy, based on the polarised *Planck* maps.
   (b) Study of the diffuse warm ionized gas in the Galaxy, based on the *Planck* map of free-free emission.
   (c) Reconstruction of the Galacto-centric distribution of emission of the different phases of the interstellar medium in the Galaxy (H_2, HI, H^+), by correlation of the *Planck* maps to tracers of each phase.
   (d) Study of the diffuse synchrotron emission from the Galaxy, in particular its spectrum and its spatial structure.
   (e) Study of the physical characteristics of the circumstellar environment of various types of stellar objects in the final phases of their evolution.
   (f) Construction and analysis of a catalogue of compact and ultra-compact HII regions and massive young stellar objects.
   (g) Construction and analysis of a catalogue of cold pre-stellar cores in the Galaxy.
   (h) Study of the spectral energy distributions of Supernova Remnants across the *Planck* bands.
   (i) Study of the spatial and spectral distribution of thermal dust polarisation to elucidate the nature of dust in the various phases of the interstellar medium.
   (j) Establishment of the spatial and spectral properties of the anomalous emission so far attributed to spinning dust particles.
   (k) Combination of *Planck* maps with lower frequency large-scale ground-based surveys to study the relationships between the various phases of the Galactic interstellar medium (atomic, molecular, ionized, relativistic, magnetic, etc.).
   (l) Study of the properties of dust in regions at high Galactic latitudes and in intermediate and high velocity clouds, using the *Planck* data in combination with other tracers such as HI, IRAS/IRIS etc.
   (m) Study of the *Planck* maps to determine the structure and distribution of mass in molecular clouds.

(n) Study of the structure and intensity of the magnetic fields (ordered and tangled components) within nearby interstellar clouds, in relation with their density and velocity structure.

6. **Solar System science**
   (a) Extraction and analysis of the zodiacal light emission, and constraints on dust properties and content within the solar system.
   (b) Detection and analysis of the emission from several classes of objects, such as main belt asteroids, planets, and comets.

It is expected that the above projects will result in around 40 scientific papers which will be submitted for publication at the time when the final scientific products are released to the community.

7. Conclusions

This paper summarises the performance of *Planck* at the time of launch in the areas most relevant for scientific analysis of the *Planck* data. It also outlines the main elements of its scientific operations and data analysis. Detailed descriptions of aspects of the payload are provided in accompanying papers in this issue. It can be concluded that:

1. The major elements of satellite and payload performance fulfill the original technical requirements.
2. The ground segment is ready for operations.
3. The *Planck* Collaboration is ready for scientific analysis.

After a flawless launch, *Planck* is now in its final orbit and has started routine surveying of the sky. There is every expectation that in-flight commissioning and performance verification activities will confirm the performance outlined here.

Acknowledgements. *Planck* is too large a project to allow full acknowledgement of all contributions by individuals, institutions, industries, and funding agencies. The main entities involved in the mission are as follows. The European Space Agency (ESA) manages the project and funds the development of the satellite, its launch, and operations. ESA's prime industrial contractor for *Planck* is Thales Alenia Space (Cannes, France). Industry from all over Europe has contributed to the development of *Planck*. Specially notable contributions to the development are due to Thales Alenia Spazio (Italy) for the Service Module, Astrium (Friedrichshafen, Germany) for the *Planck* reflectors, and Oerlikon Space (Zürich, Switzerland) for the payload structures. Much of the most challenging cryogenic and optical testing has been carried out at the Centre Spatial de Liège in Belgium and on the premises of Thales Alenia Space in Cannes. Two Consortia, comprising around 50 scientific institutes within Europe and the US, and funded by agencies from the participating countries, have developed the scientific instruments LFI and HFI, and delivered them to ESA (see also Appendix A). The Consortia are also responsible for scientific operation of their respective instruments and processing the acquired data. The Consortia are led by the Principal Investigators: J.-L. Puget in France of HFI (funded principally via CNES) and N. Mandolesi in Italy of LFI (funded principally via ASI). NASA has funded the US *Planck* Project, based at JPL and involving scientists at many US institutions, which has contributed very significantly to the efforts of these two Consortia. A Consortium of Danish institutes (DK-Planck), funded by the Danish National Research Council, has participated with ESA in a joint development of the two reflectors for the *Planck* telescope. The author list for this paper has been selected by the *Planck* Science Team, and is composed of individuals from all of the above entities who have made multi-year contributions to the development of the mission. It does not pretend to be inclusive of all contributions.

Appendix A: The *Planck* Scientific Collaboration

The *Planck* Scientific Collaboration consists of all the scientists which have contributed to the development of the *Planck* mission, and who will participate in the scientific exploitation of the *Planck* data during the proprietary period, which nominally ends with the release of the scientific products to the community 3.5 yr after launch, i.e. in January 2013. They are members of one or more among four Consortia of scientists:

1. The LFI Consortium, Principal Investigator N. Mandolesi of the Istituto di Astrofisica Spaziale e Fisica Cosmica (Bologna, Italy), includes the following participating institutes:
   – ASI - Agenzia Spaziale Italiana, Roma (Italy)
   – CNR - Istituto di Fisica del Plasma, Milano (Italy)
   – Centre d'Étude Spatiale des Rayonnements, Toulouse (France)
   – Computational Research Division, LBNL, Berkeley CA (USA)
   – Danish Space Research Institute, Copenhagen (DK)
   – DICOM, Universidad de Cantabria, Santander (Spain)
   – Haverford College, Haverford PA (USA)
   – Helsinki Institute of Physics, Helsinki (Finland)
   – INAF - IASF-Bo, Bologna (Italy)
   – INAF - IASF-Mi Milano (Italy)
   – INAF - Istituto di Radioastronomia (Italy)
   – INAF - Osservatorio Astronomico di Arcetri, Firenze (Italy)
   – INAF - Osservatorio Astronomico di Bologna, Bologna (Italy)
   – INAF - Oss. Astronomico di Padova, Padova (Italy)
   – INAF - Oss. Astronomico di Trieste, Trieste (Italy)
   – INFN - sezione di Trieste, Trieste (Italy)
   – INFN - sezione di Tor Vergata, Roma (Italy)
   – Institute for Space Science, Bucharest-Magurele (Romania)
   – Instituto de Física, Universidad de Cantabria, Santander (Spain)
   – Institute of Theoretical Astrophysics, University of Oslo (Norway)
   – Instituto de Astrofísica de Canarias (Spain)
   – Integral Science Data Centre, University of Geneva, Versoix (Switzerland)
   – Jet Propulsion Laboratory, Pasadena (USA)
   – Jodrell Bank Centre for Astrophysics, The University of Manchester, Manchester (UK)
   – Lawrence Berkeley National Laboratory, Berkeley (USA)
   – Metsahövi Radio Observatory, Helsinki (Finland)
   – Millilab, VTT Information Technology, Espoo (Finland)
   – Max-Planck Institut für Astrophysik, Garching (Germany)
   – National Radio Astronomy Observatory, Charlottesville VI (USA)
   – Research and Scientific Support Dpt, European Space Agency -ESTEC, Noordwijk (The Netherlands)
   – SISSA/ISAS - Astrophysics Sector, Trieste (Italy)
   – Space Sciences Laboratory, University of California, Berkeley (USA)
   – Università degli Studi di Milano - Dipartimento di Fisica, Milano (Italy)
   – Università degli Studi di Roma Padova - Dipartimento di Fisica, Padova (Italy)
   – Università degli Studi di Roma "Tor Vergata" - Dipartimento di Fisica, Roma (Italy)
   – Università degli Studi di Trieste - Dipartimento di Fisica, Trieste (Italy)
   – University of British Columbia, Vancouver (Canada)

- University of California at Berkeley, Physics Department, Berkeley (USA)
- University of California at Santa Barbara, Physics Department, Santa Barbara (USA)
- University of Helsinki, Physics Department, Helsinki (Finland)
- University of Oxford, Nuclear and Astrophysics Laboratory, Oxford (UK)

2. The HFI Consortium, Principal Investigator J.-L. Puget of the Institut d'Astrophysique Spatiale (Orsay, France), and co-PI F.R. Bouchet of the Institut d'Astrophysique de Paris (Paris, France), includes the following participating institutes:
   - Cardiff University, School of Physics and Astronomy, UK
   - CEA, CE Saclay, IRFU/Service de Physique des Particules, Gif-sur-Yvette, France
   - Dipartimento di Fisica, Università La Sapienza, Roma, Italy
   - CESR, Centre d'Étude Spatiale des Rayonnements, CNRS, Toulouse, France
   - CNES, Paris, France
   - CNES, Toulouse, France
   - Department of Experimental Physics, National University of Ireland (NUI), Maynooth, Ireland
   - Department of Physics (Cavendish Laboratory), University of Cambridge, UK
   - Department of Physics, California Institute of Technology, Pasadena, USA
   - European Space Agency - ESTEC, Astrophysics Division, Noordwijk, The Netherlands
   - European Space Astronomy Centre, Villanueva de la Cañada, Madrid, Spain
   - IAS, Institut d'Astrophysique Spatiale, CNRS & Université Paris 11, Orsay, France
   - IAP, Institut d'Astrophysique de Paris, CNRS, Paris, France
   - Institut Néel, CNRS, Univ. Joseph Fourier Grenoble I, Grenoble, France
   - Institute of Astronomy, University of Cambridge, Madingley Road, Cambridge CB3 OHA, UK
   - Institute of Radiophysics and Electronics, NAS of Ukraine, Kharkov, Ukraine
   - Jet Propulsion Laboratory, California Institute of Technology, Pasadena, USA
   - Kavli Institute for Particle Astrophysics and Cosmology and Department of Physics, Stanford University, Stanford, USA
   - Laboratoire Astroparticule et Cosmologie (APC), CNRS & Université Paris Diderot - Paris 7, Paris, France
   - Laboratoire d'Astrophysique de Grenoble (CNRS, UMR 5571) 414 rue de la piscine, Grenoble, France
   - LAL, Laboratoire de l'Accélerateur Linéaire, CNRS & Université Paris 11, Orsay, France
   - Laboratoire de Physique Subatomique et de Cosmologie (LPSC), Univ. Joseph Fourier Grenoble I, CNRS/IN2P3, Institut National Polytechnique de Grenoble, Grenoble, France
   - LERMA, CNRS, Observatoire de Paris, Paris, France
   - Optical Science Laboratory, University College London (UCL), London, UK
   - Princeton University, Department of Physics, Joseph Henry Laboratory, USA
   - Royal Observatory Edinburgh, Edinburgh, UK
   - STFC, Rutherford Appleton Laboratory, Harwell Science and Innovation Campus, Didcot, UK
   - SUPA, Institute of Astronomy, University of Edinburgh, Edinburgh, UK
   - The University of Manchester, JBCA, School of Physics and Astronomy, UK
3. The DK-Planck Consortium, led by H.U. Norgaard-Nielsen of the Danish National Space Institute (Copenhagen, Denmark), includes the following participating institutes:
   - Danish National Space Institute, Copenhagen (Denmark)
   - Niels Bohr Institute, Copenhagen (Denmark)
   - Theoretical Astrophysics Centre, Copenhagen (Denmark)
4. ESA's *Planck* Science Office, Project Scientist J. A. Tauber.

The *Planck* Science Team (see membership at http://www.rssd.esa.int/Planck) is a formal body set up by ESA at the inception of the project to represent the scientific interests of the mission, which has had a key advisory role vis-à-vis the development of the satellite, payload and ground segment. It is a recognised principle of the mission that the scientific exploitation of *Planck* during the proprietary period is a joint venture between the involved Consortia, and the Science Team is the body which has taken the role to organise, plan, coordinate, and oversee all the common activities in this respect. All members of the *Planck* Scientific Collaboration have agreed to abide by the policies set by the Science Team with regard to data access and publication of scientific results. A complete online database of all members of the *Planck* Collaboration is maintained at http://www.rssd.esa.int/index.php?project=IDIS&page=people.

References

Aumont, J., Conversi, L., Falgarone, E., et al. 2010, A&A, 514, A70
Ade, P. A. R., Savini, G., Sudiwala, R., et al. 2010, A&A, 520, A11
Bhandari, P., Prina, M., Bowman, R. C. Jr., et al. 2004, Sorption Coolers Using A Continuous Cycle To Produce 20 K For The Planck Flight Mission, Cryogenics, 44, 395
Benoît, A., Sirbi, A., Bradshaw, T., et al. 1997, in 6th European Symposium on Space Environmental Control Systems, ed. T. D. Guyenner, ESA SP, 400, 497
Bersanelli, M., Bouchet, F. R., Efstathiou, G., et al. 1996, Report on the Phase A Study of COBRAS/SAMBA, ESA Publication D/SCI(96)3
Bersanelli, M., Muciaccia, P. F., Natoli, P., Vittorio, N., & Mandolesi, N. 1997, A&AS, 121, 393
Bersanelli, M., Mandolesi, N., Butler, R. C., et al. 2010, A&A, 520, A4
Bradshaw, T., et al. 1997, in 6th European Symposium on space environmental control systems, held in Noordwijk, The Netherlands, 20–22 May, ed. T.-D. Guyenne; European Space Agency, SP-400, 465
Boggess, N. W., Mather, J. C., Weiss, R., et al. 1992, ApJ, 397, 420
Burigana, C., Gruppuso, A., & Finelli, F. 2006, MNRAS, 371, 1570
Cappellini, B., Maino, D., & Bersanelli, M. 2003, A&A, 409, 375
Couchot, F., Delabrouille, J., Kaplan, J., & Revenu, B. 1999, A&AS, 135, 579
Delabrouille, J., Puget, J.-L., Gispert, R., & Lamarre, J.-M. 2000, Ap. Lett. & Comm., 37, 259
Dupac, X., & Tauber, J. 2005, A&A, 430, 363
Fixsen, D. J., Cheng, E. S., Gales, J. M., et al. 1996, ApJ, 473, 576
Górski, K. M., Eric Hivon, A. J., Banday, B. D., et al. 2005, ApJ, 622, 759
Hamaker, J. P., & Leahy, J. P. 2004, A study of CMB differencing polarimetry with particular reference to Planck, ESA Report SCI-A/2003.312/JT
Hinshaw, G. Weiland, J. L., Hill, R. S., et al. 2009, ApJS, 180, 225
Holmes, W. A., Bock, J. J., Crill, B. P., et al. 2008, Appl. Opt., 47, 5996
Huffenberger, K. M., Crill, B. P., Lange, A., et al. 2010, A&A, 510, A58
Keihänen, E., Kurki-Suonio, H., & Poutanen, T. 2005, MNRAS, 360, 390
Lamarre, J.-M., Puget, J.-L., Ade, P. A. R., et al. 2010, A&A, 520, A9
Leahy, J. P., Bersanelli, M., D'Arcangelo, O., et al. 2010, A&A, 520, A8
Leach, S. M., Cardoso, J.-F., Baccigalupi, C., et al. 2008, A&A 491, 597
Maffei, B., Noviello, F., Murphy, J. A., et al. 2010, A&A, 520, A12
Maino, D., Burigana, C., Gorski, K. M., Mandolesi, N., & Bersanelli, M. 2002, A&A, 387, 356

Mandolesi, N., & Smoot, G. F. 1993, Proposal for COBRAS – the Cosmic Background Anisotropy Satellite, submitted to ESA in 2003 in answer to the M3 call for mission ideas
Mandolesi, N., Bersanelli, M., Butler, R. C., et al. 2010, A&A, 520, A3
Maris, M., Maino, D., Burigana, C., et al. 2004, A&A 414, 777
Maris, M., Tomasi, M., Galeotta, S., et al. 2009, JINST, 4, T12018
Meinhold, P., Leonardi, R., Aja, B., et al. 2009, JINST, 4, T12009
Mennella, A., Bersanelli, M., Butler, R. C., et al. 2010, A&A, 520, A5
Pajot, F., Ade, P. A. R., Beney, J.-L., et al. 2010, A&A, 520, A10
Pearson, D., Zhang, B., Prina, M. 2006, Flight Acceptance Testing of the Two JPL Planck Sorption Coolers, Cryocoolers 14 (ICC Press), 497
Piat, M., Lagache, G., Bernard, J.-P., et al. 2002, A&A, 393, 359
Planck Collaboration 2005, Planck: The Scientific Programme, ESA publication ESA-SCI(2005)/01
Puget, J. L. 1993, Proposal for SAMBA - the SAtellite for Measurements of Background Anisotropies, submitted to ESA in 2003 in answer to the M3 call for mission ideas
Reix, J. M., Collaudin, B., Rideau, P., et al. 2007, in Proceedings of the 2007 Congress of the International Astronautical Federation, paper IAC-07-A3.I.A.23
Rosset, C., Tristram, M., Ponthieu, N., et al. 2010, A&A, 520, A13
Sandri, M., Villa, F., Bersanelli, M., et al. 2010, A&A, 520, A7
Tauber, J. A., Norgaard-Nielsen, H.-U., Ade, P. A. R., et al. 2010, A&A, 520, A2
Triqueneaux, S., Sentis, L., Camus, P., Benoit, A., & G. Guyot 2006, Cryogenics, 46, 288
Tristram, M. 2005, Ph. D. Thesis, Université Joseph Fourier, Grenoble 1
Villa, F., Terenzi, L., Sandri, M., et al. 2010, A&A, 520, A6

[1] Agenzia Spaziale Italiana Science Data Center, c/o ESRIN, via Galileo Galilei, Frascati, Italy
[2] Agenzia Spaziale Italiana, viale Liegi 26, Roma, Italy
[3] Astrium GmbH, Friedrichshafen, Germany
[4] Astroparticule et Cosmologie, CNRS (UMR7164), Université Denis Diderot Paris 7, Bâtiment Condorcet, 10 rue A. Domon et Léonie Duquet, Paris, France
[5] Astrophysics Sector, SISSA-ISAS, via Beirut 4, Trieste, Italy
[6] Cardiff University, Dept. of Physics and Astronomy, Queens Buildings, 5 The Parade, Cardiff, Wales, UK
[7] CEA Saclay, IrfU/SAp, Gif-sur-Yvette, France
[8] CEA Saclay, IrfU/SPP Bat 141, Gif-sur-Yvette, France
[9] Centre d'Étude Spatiale des Rayonnements, UMR 5187, 9 Av. du Colonel Roche, Toulouse, France
[10] Centre of Mathematics for Applications, University of Oslo, Blindern, Oslo, Norway
[11] Centre Spatial de Liège, Liège Science Park, Av. du Pré-Aily, Angleur, Belgium
[12] CESR, CNRS-Université de Toulouse, 9 Av. du Colonel Roche, Toulouse, France
[13] CITA, University of Toronto, McLennan Labs 60, St. George St., Toronto, Canada
[14] CNES, Centre Spatial de Toulouse, 18 avenue Edouard Belin, Toulouse, France
[15] CNR - ISTI, Area della Ricerca, via G. Moruzzi 1, Pisa, Italy
[16] Departament de Teoria del Senyal i Comunicacions, Universitat Politécnica de Catalunya, Campus Nord, Edificio D4, C. Jordi Girona, 1-3, Barcelona, Spain
[17] Departamento de Física, Universidad de Oviedo, Avda. Calvo Sotelo s/n, Oviedo, Spain
[18] Departamento de Ingeniería de Comunicaciones, Universidad de Cantabria, Plaza de la Ciencia, Santander, Spain
[19] Department of Physics & Astronomy, University of British Columbia, 6224 Agricultural Road, Vancouver, British Columbia, Canada
[20] Department of Physics and Astronomy, University of Southern California, Los Angeles, California, USA
[21] Department of Physics, Gustaf Hällströmin katu 2a, University of Helsinki, Helsinki, Finland
[22] Department of Physics, Princeton University, Princeton, New Jersey, USA
[23] Department of Physics, Purdue University, 525 Northwestern Avenue, West Lafayette, Indiana, USA
[24] Department of Physics, Standford University, Stanford, California, USA
[25] Department of Physics, University of California, Berkeley, California, USA
[26] Department of Physics, University of California, One Shields Avenue, Davis, California, USA
[27] Department of Physics, University of California, Santa Barbara, California, USA
[28] Department of Physics, University of Illinois at Urbana-Champaign, 1110 West Green Street, Urbana, Illinois, USA
[29] Department of Physics, University of Oxford, 1 Keble Road, Oxford, UK
[30] Departments of Astronomy and Physics, University of California, Berkeley, California, USA
[31] Dipartimento di Fisica "G. Galilei", Università degli Studi di Padova, via Marzolo 8, Padova, Italy
[32] Dipartimento di Fisica, Università degli Studi di Milano, via Celoria, 16, Milano, Italy
[33] Dipartimento di Fisica, Università di Roma Tor Vergata, via della Ricerca Scientifica, 1, Roma, Italy
[34] Dipartimento di Fisica, Università La Sapienza, P. le A. Moro 2, Roma, Italy
[35] DTU Space, National Space Institute, Juliane Mariesvej 30, Copenhagen, Denmark
[36] European Space Agency, Astrophysics Division, ESTEC, Keplerlaan 1, 2201AZ Noordwijk, The Netherlands
e-mail: jtauber@rssd.esa.int
[37] European Space Agency, Herschel-Planck Project, ESTEC, Keplerlaan 1, Noordwijk, The Netherlands
[38] European Space Agency, Herschel-Planck Project, European Space Operations Centre – ESOC, Robert-Bosch-Str. 5, Darmstadt, Germany
[39] European Space Agency, Planck Science Office – ESAC, Camino bajo del Castillo, s/n, Urbanización Villafranca del Castillo, Villanueva de la Cañada, Madrid, Spain
[40] Física Teórica y del Cosmos, Universidad de Granada, Granada, Spain
[41] Haverford College Astronomy Department, 370 Lancaster Avenue, Haverford, Pennsylvania, USA
[42] Helsinki Institute of Physics, Gustaf Hällströmin katu 2, University of Helsinki, Helsinki, Finland
[43] Imperial College London, Astrophysics group, Blackett Laboratory, Prince Consort Road, London, UK
[44] INAF - Arcetri Astrophysical Observatory, Largo Enrico Fermi 5, Florence, Italy
[45] INAF - Istituto di Astrofisica Spaziale e Fisica Cosmica, via Gobetti 101, Bologna, Italy
[46] INAF - Osservatorio Astronomico di Trieste, via G.B. Tiepolo 11, Trieste, Italy
[47] INAF Osservatorio Astrofisico di Catania, via S. Sofia, Catania, Italy
[48] INAF/IASF Milano, via E. Bassini 15, Milano, Italy
[49] INAF - Osservatorio Astronomico di Padova, Vicolo dell'Osservatorio 5, Padova, Italy
[50] Infrared Processing and Analysis Center, California Institute of Technology, Pasadena, California, USA
[51] Institut d'Astrophysique de Paris, CNRS UMR7095, & UPMC, Université Pierre & Marie Curie, 98bis boulevard Arago, Paris, France
[52] Institut d'Astrophysique Spatiale, CNRS (UMR8617) Université Paris-Sud 11, Bâtiment 121, Orsay, France
[53] Institut Néel, CNRS, Université Joseph Fourier Grenoble I, 25 rue des Martyrs, Grenoble, France
[54] Institute for Space Sciences, Bucharest-Magurale, Romania
[55] Institute of Astronomy and Astrophysics, Academia Sinica, Taipei, Taiwan
[56] Institute of Theoretical Astrophysics, University of Oslo, Blindern, Oslo, Norway

[57] Instituto de Astrofísica de Canarias, C/vía Láctea s/n, La Laguna, Tenerife, Spain
[58] Instituto de Física de Cantabria (CSIC-Universidad de Cantabria), Avda. de los Castros s/n, Santander, Spain
[59] ISDC Data Centre for Astrophysics, University of Geneva, ch. d'Ecogia 16, Versoix, Switzerland
[60] Istituto di Fisica del Plasma, CNR, via Roberto Cozzi 53, Milano, Italy
[61] Jet Propulsion Laboratory, California Institute of Technology, 4800 Oak Grove Drive, Pasadena, California, USA
[62] Jodrell Bank Centre for Astrophysics, School of Physics & Astronomy, University of Manchester, Manchester, UK
[63] Laboratoire de l'Accélerateur Linéaire, Université Paris-Sud, CNRS/IN2P3, Orsay, France
[64] Laboratoire d'Astrophysique de Grenoble (CNRS, UMR 5571), 414 Rue de la piscine, Grenoble, France
[65] Lawrence Berkeley National Laboratory, Berkeley, California, USA
[66] LERMA, CNRS, Observatoire de Paris, 61 Avenue de l'Observatoire, Paris, France
[67] Max Planck Institut für Astrophysik, Karl-Schwarzschild-Str. 1, Garching, Germany
[68] Metsähovi Radio Observatory, Helsinki University of Technology, Metsähovintie 114, Kylmälä, Finland
[69] MilliLab, VTT Information Technology, Tietotie 3, Espoo, Finland
[70] National University of Ireland (NUI), Department of Experimental Physics, Maynooth, Co. Kildare, Dublin, Ireland
[71] Niels Bohr Institute, Blegdamsvej 17, Copenhagen, Denmark
[72] Observatory, Tähtitorninmäki, University of Helsinki, Helsinki, Finland
[73] Oerlikon Space, Schaffhauserstrasse 580, Zürich, Switzerland
[74] Officine Pasquali, via Del Palazzo dei Diavoli 124, Firenze, Italy
[75] Optical Science Laboratory, University College London, Gower Street, London, UK
[76] Research and Scientific Support Department of ESA, ESTEC, Noordwijk, The Netherlands
[77] Rutherford Appleton Laboratory, Chilton, Didcot, UK
[78] Sener Ingeniería y Sistemas S.A., C. Severo Ochoa (Parq. Tecnológico De Madrid) 4, Tres Cantos, Spain
[79] Space Sciences Laboratory, University of California, Berkeley, California, USA
[80] Spitzer Science Center, 1200 E. California Blvd., Pasadena, California, USA
[81] Telecommunication and System Engineering Department, Universitat Autònoma de Barcelona (UAB), Barcelona, Spain
[82] Thales Alenia Space France, 100 Boulevard du Midi, Cannes la Bocca, France
[83] Thales Alenia Space Italia, Collegno 253, Turin, Italy
[84] Thales Alenia Space Italia, S.S. Padana Superiore, 290, Vimodrone, Milano, Italy
[85] TICRA, Laederstraede 34, Copenhagen, Denmark
[86] Tycho Brahe Planetarium, Gl. Kongevej 10, Copenhagen, Denmark
[87] University of Barcelona, ICE/CSIC, Torre c5, par-2, Cerdanyola (Barcelona), Spain
[88] University of California, Computational Research Department, Lawrence Berkeley National Laboratory, Berkeley, California, USA
[89] University of Cambridge, Cavendish Laboratory, Astrophysics group, J J Thomson Avenue, Cambridge, UK
[90] University of Cambridge, Institute of Astronomy, Madingley Road, Cambridge, UK
[91] University of Granada, Departamento de Física Teórica y del Cosmos, Facultad de Ciencias, Granada, Spain
[92] University of Miami, Knight Physics Building, 1320 Campo Sano Dr., Coral Gables, Florida, USA
[93] University of Trieste, Department of Physics, via A. Valerio 2, Trieste, Italy
[94] Ylinen Electronics Ltd., Teollisuustie 9A, Kauniainen, Finland
[95] Zentrum für Astronomie, Universität Heidelberg, Institut für Theoretische Astrophysik, Albert-Ueberle-Str. 2, Heidelberg, Germany
[96] LPSC, Université Joseph Fourier Grenoble I, CNRS/IN2P3, Institut National Polytechnique de Grenoble, 53 avenue des Martyrs, 38026 Grenoble Cedex, France